Material Parameter Identification by Means of Depth-Sensing Micro-Indentation, FE Simulation and Optimization

(押込み深さ検知マイクロインデンテーション，有限要素シミュレーションおよび最適化法を用いた材料パラメータ同定)

2005年

濱崎　洋

Material Parameter Identification by Means of Depth-Sensing Micro-Indentation, FE Simulation and Optimization

(押込み深さ検知マイクロインデンテーション，有限要素シミュレーションおよび最適化法を用いた材料パラメータ同定)

Department of Mechanical System Engineering,
Graduate School of Engineering, Hiroshima University

D1381005　Hiroshi Hamasaki

広島大学大学院工学研究科
機械システム工学専攻博士課程後期

D1381005　濱崎　洋

Contents

Chapter 1: Introduction

1.1 Micro-indentation

The depth-sensing micro-indentation test, where a small tip of indenter penetrates into a material surface, reveals tremendous information of material characteristics [1-5]. This technique is especially suitable for small specimens such as jointed solder alloys, welded materials, thin films and coatings which volumes are not large enough to be formed as a specimen for conventional uniaxial tension and compression tests. A schematic illustration of indentation profile with a conical indenter is shown in Fig. 1-1. Indentation load (P)-depth (h) response (see schematic illustration, Fig. 1-2), which is continuously recorded during the indentation process, is important information to determine mechanical properties of materials. In the loading process, load P increases with indenter penetration h up to the maximum load P_{max} (A in Fig. 1-1). Then, P_{max} is kept constant in a certain holding time, where indentation creep (h^{creep}) , *i.e.*, the progress of indenter penetration h, takes place and it reaches the maximum depth (h_{max}) (B in Fig. 1-1 and Fig. 1-2). Elastic penetration recovery (h^e) is observed during unloading process, and the residual penetration (h^p) and residual deformation radius a can be measured by microscopy after the indenter is completely unloaded (C in Fig. 1-1 and Fig. 1-2).

In this thesis, we propose a material parameter identification method using depth-sensing micro-indentation [6,7]. For this purpose, the inverse approach based on a curve fitting technique between experimental data and numerical simulation results is adopted. FE simulation is selected for a numerical simulation tool because it is commonly recognized as the most accurate method to deal with a nonlinear structural analysis with respect to a contact problem. In the inverse approach, an optimization technique, which achieves an automatic parameter identification system, is introduced. One of the serious problems is that the optimization process requires a large number of iterative FE simulation, hence the total computing time to obtain the optimal solution becomes significantly large. To solve this problem, a new algorithm of high- and low-fidelity modeling is employed. Varieties of materials are dealt with in this work, such as elastic-plastic and viscoplastic materials; homogeneous bulk materials and heterogeneous materials; and coatings placed on substrates. Especially for multi-phase materials and coatings, the guidelines for appropriate indenter-penetration depth are investigated [8-10].

In the following sections, the review of conventional hardness tests and analytical works on micro-indentation are summarized. Furthermore, further necessary tasks to establish the inverse approach to the identification of material parameters based on the depth-sensing micro-indentation technique are described. Subsequently, the purpose of the present work and the contents of this thesis are indicated.

1.2 Review of previous research works on micro-indentation

1.2.1 Hardness tests

Hardness tests, such as Vickers, Knoop, Brinell and Rockwell tests [11], are very popular to measure the *hardness* of metallic materials. From these tests, the hardness value (calculated in Eq. (1-1)) is determined

as

$$H = \frac{P}{A} \tag{1-1}$$

where H is the hardness value, P is the load and A is the indenter-contact or projected area. Various hardness tests had been standardized as listed in Table 1-1. Here, it should be noted that area A in Eq. (1-1) is either indenter-contact area or projected area depending on the type of hardness tests. For example, the indenter-contact area is used for Vickers and Brinell tests, while the projected area for Meyer and Knoop hardness tests. The herdness H vs. yield strength σ_Y relationship was empirically found by Tabor [12, 13], while the theoretical works by Hill *et al.* [14] and Storåkers and Larsson [15] confirmed the Tabor's relationship:

$$H \approx 2.8\sigma_Y \tag{1-2}$$

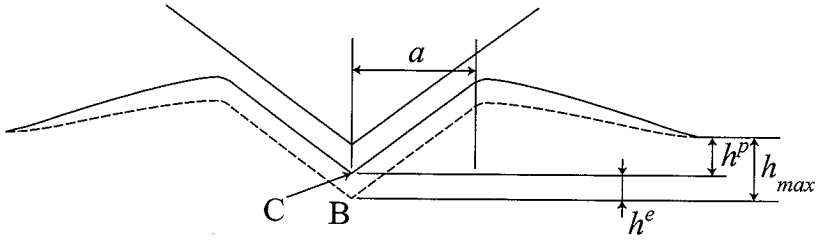

Fig. 1-1 Schematic illustration of indentation profile in the case of conical indentation.

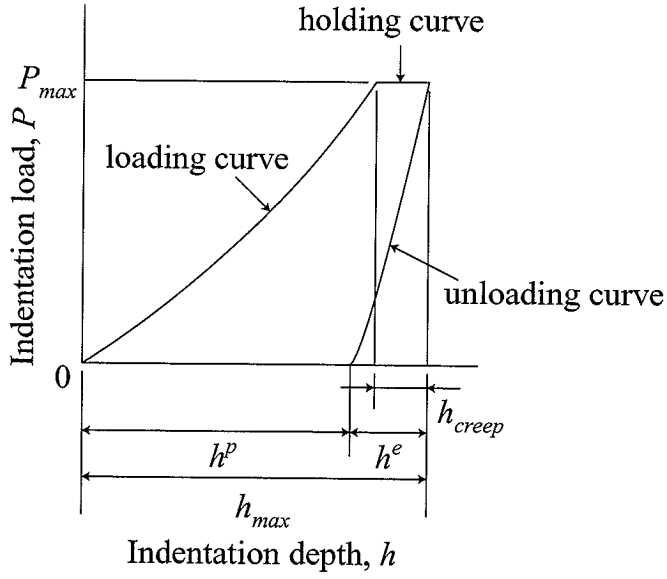

Fig. 1-2 Illustration of typical indentation load (P) vs. depth (h) curve.

Table 1-1 Static indentation tests.

Name of test	nominal load (kgf)	indenter	hardness formula*
Brinell hardness test	500-300	spherical, steel	$H=\frac{2P}{\pi D\left[D-\left(D^2-d^2\right)^{1/2}\right]}$
Vickers hardness test	less than 120	diamond pyramid with square base (apex angle 136°)	$H_V=1.8544\frac{P}{d^2}$
Rockwell hardness test	less than 150	diamond cone with a spherical tip	$H=\frac{4P}{\pi d^2}$
Berkovich test (micro-hardness)	0.005-3	diamond pyramid with a triangular base (angle between the vertical axis and the facet 65°)	$H=\frac{1570P}{l^2}$
Knoop test (micro-hardness)	0.005-3	diamond pyramid with a square base	$H_K=\frac{P}{7.028\times10^{-3}d_1^2}$

* P: applied load; D: diameter of spherical indenter; d: diameter of the impression; d_1: the lengths of the long diagonal of the indent and the perpendicular distance from a corner to the opposite base of the triangular impression.

1.2.2 Elastic contact problem and determination of Young's modulus

The elastic contact problem between two spheres which have different radii was solved by Hertz [16]. In his theory, the maximum pressure, radius of contact surface and displacement between the centers of spheres are expressed by the indentation load, radii of spheres and elastic properties (Young's modulii and Poisson's ratios of spheres). For an elastic material, Bulychew [17] proved that the slope of P-h curve is proportional to the effective modulus E_{eff}, which is calculated by Hertz contact theory (Eq. 1-1) and squared root of projected area for cylindrical, conical and spherical indentations:

$$\frac{1}{E_{eff}}=\frac{1-\nu_1^2}{E_1}-\frac{1-\nu_2^2}{E_2} \tag{1-1}$$

where E and ν denote Young's modulus and Poisson's ratio respectively, and subscripts 1 and 2 indicate these spheres. Based on that, Doerner and Nix [18] and Oliver and Pharr [19, 20] provided the identification procedure of Young's modulus, where only unloading part of P-h curve obtained form a self-similar indentation is used, with the assumption that an indentation recovery during the unloading process consists only of elastic deformation. This method has been widely applied on many materials (see [21, 22]). Another method of measurement of Young's modulus has been proposed by Field and Swain [23-25]. They used the stepwise indentation with the multiple partial-unloading of a spherical indentation to calculate the effective modulus using Hertz equation.

1.2.3 Material parameter identification using micro-indentation

(a) Plasticity parameter identification

Many research works has been performed to describe the mechanism of depth-sensing micro-indentation and to obtain plasticity parameters of workhardening materials. The first attempt to determine the plasticity parameters was made by Meyer [26]. Later, O'Neill [27] and Hill [14] have driven the relationship between the hardness value for spherical indentation and workhardening coefficient n in a power low stress-strain relationship $\sigma = C(\varepsilon^p)^n$:

$$H = \frac{P}{\pi a^2} = \alpha \beta^n C \left(\frac{a}{D} \right)^n \tag{1-2}$$

where α and β are the constants with values of 2.8 and 0.4, respectively and D denotes the diameter of a spherical indenter. Plasticity parameters C and n can be identified by measuring the variation of P with respect to a, where a is measured in the unloaded configuration. Slope of a $\log(P/\pi a^2)$-$\log(a/D)$ curve equals to power law exponent n. For the contact pressure, Matthews [28] suggested that the pressure distribution between a rigid sphere and a flat material, which stress-strain curve follows the power law relationship $\sigma = C(\varepsilon^p)^n$, is dependent on workhardening exponent n, Hill [14] later corrected this form and presented the following equation so as to have more realistic pressure distribution even for non-hardening materials:

$$p(r) = \left(1 + \frac{s}{2} \right) \left(1 - \frac{r^2}{a^2} \right)^{\frac{s}{2}} \frac{P}{\pi a^3} \tag{1-3}$$

where $p(r)$ is the contact pressure which is given as a function of the distance r from the center of indentation profile in horizontal direction, and s is the material parameter obtained from workhardening exponent n.

As to 'pile-up' and 'sink-in' phenomena, Norbury and Samuels [29] measured the spherical indentation profiles and found that the ratio of the height at the edge of an indentation profile to residual depth B depends only on workhardening exponent n and was independent of load P, that means this height to depth ratio is constant during the spherical indentation. An analytical form to evaluate this constant value is achieved by Hill [14]:

$$B = \left(\frac{2-n}{4+n} \right) \left(2 + \frac{s}{2} \right) \tag{1-4}$$

Since, in spherical indentation, the diameter of a residual indentation profile after unloading is larger than that of its indenter due to the elastic recovery, Eq. (1-2) is valid only when a/D has a small value. On the contrary, Eq. (1-4) is valid only when the deformation of the material under the indenter is fully plastic. Adler [30, 31] and Kucharski *et al.* [32-34] made precise analysis of contact diameter and suggested that the diameter of indentation profile can be separated into elastic and plastic diameter. By applying Eq. (1-2) to the plastic part of the diameter of indentation contact profile, they proposed analytical methods to

identify the workhardening exponent n and coefficient C in power-law constitutive model. However, such analytical models contain several assumptions, which cause error in obtained material parameters.

(b) Viscoplasticity parameter identification

Several attempts to determine viscoplastic parameters were made [35-38] based on the dimensional analysis of self-similar indentation for creep material proposed by Sargent and Ashby [39]. They found that $1/n$, where n is the rate sensitivity exponent in a strain rate-stress constitutive model, and activation energy Q can be obtained from self-similar indentation creep tests under constant load P, namely, n equals to the linear slope the $\log(dH/Hdt)$-$\log(1/t)$ curve, and Q the slope of $\log(H/G)$-(T_m/T) curve (G: shear modulus of elasticity; T_m: melting point). Ogawa *et al.* [35, 36] applied this method to determine the rate sensitivity exponent of solder alloys. Fujiwara [37] and Fujiwara-Otsuka [38] developed a high-temperature indentation apparatus and obtained the rate sensitivity exponent and activation energy of solder alloys. Ma and Yoshida [40-42] determined the rate sensitivity exponent from the work of indentation creep during load-hold part of P-h curve. In these methods, where only indentation-creep data (progressive indenter penetration vs. time under a constant load) are exclusively considered, many indentations with different levels of indentation-creep loads are required to determine the rate sensitivity exponent n of a material. Instead, if a loading part of P-h curve (O $\rightarrow$ A in Fig. 1-2) is considered together with the indentation creep, the required number of indentation tests can be reduced.

(c) Parameter identification for coating material

Micro-indentation has been employed to determine the mechanical properties of thin films and coatings. For example, Nowak *et al.* [43, 44] calculated P-h curves for HfN and GaN films using FE simulation. Yu *et al.* [45] obtained Young's modulus of GaN film from Hertz contact theory. However, limited numbers of research works are found for the parameter identification of coating. Leouvier *et al.*, [46, 47] found that if the indentation depth is ten times smaller than the thickness of coating, the effect of deformation of its substrate is negligibly small for a case that the yield strength differential between coating and thickness $Y_c/Y_s > 10$ (Y_c and Y_s denote yield strengths of coating and thickness, respectively), while for the case of $Y_c/Y_s < 10$, one-tenth rule is violated for a self-similar indentation. Sun *et al.* [48] performed FE simulation of micro-indentation with a conical indenter having a rounded tip-top (its radius was 1 μm), and led the preferable ratio of coating thickness to indenter-penetration depth as a polynomial function of yield strength differential Y_c/Y_s to remove the effect of substrate deformation from a P-h curve. However, all the above investigations performed only for a indenter with a rounded tip, but not for a fully spherical indenter and self-similar indenters with sharp tips (e.g., Berkovich, Vickers and conical indenters).

1.2.4 Parameter identification as an optimization problem

Many research works on material parameter identification based on inverse approach has been performed [49-54]. Toropov *et al.* [49] proposed a methodology of material parameter identification based on curve fitting technique, where the discrepancy between an experimentally obtained mechanical response (*e.g.* stress-strain curve of uniaxial tension test) and the corresponding numerical result (*e.g.* FE simulation result) is minimized by iteratively correcting the material parameters in the numerical simulation. As an

example of its application, Yoshida *et al.* [50] determined plasticity parameters of a stainless steel sheet and mild steel sheet in a constitutive model. As for the inverse approach for micro-indentation, Nakamura *et al.* [51, 52], Rikards *et al.* [53] and Constantinescu *et al.* [54] performed parameter identification by fitting *P-h* curves between experimental result and FE simulation for functionally graded materials and polymers. However, almost no application of this technique for metals is found. Moreover, since this technique requires a large number of FE simulations until a proper set of material parameters are found, the development of optimization technique which reduces the total computing time of optimization process is necessary.

1.3 Purpose and content of present work

As mentioned in the above review, the depth-sensing micro-indentation has already been widely recognized as a convenient mechanical test for small-volume materials. However, there is still lack of research on the material parameter identification using micro-indentation. Problems to be investigated are as follows:

(1) Since the micro-indentation is not an experiment for direct measurement of stress-strain curve of a material, several methods have been proposed for the identification of material parameters in a constitutive model. However, these methods have been constructed only for specific types of constitutive model such as Ludwik-type plasticity and Norton-type creep law. Therefore, a material parameter identification method which can apply to any types of constitutive model is required.

(2) Material parameter identification methods based on simplified analytical models of micro-indentation would not accurately enough since the analytical results have a certain errors because of their simplified modeling. To overcome this problem, accurate FE simulation should be employed for material parameter identification.

(3) For a multi-phase material, if we want to determine the mechanical properties of its individual phases, it is important to have a guideline for an appropriate indenter-penetration depth, because if the indentation is too deep, *P-h* response would include the effect of deformation of the other neighboring phases. This is also essential for coating/substrate systems.

(4) In the inverse approach, where the difference of *P-h* curves between experimental data and FE simulation result is minimized, numbers of iterations are necessary. The problem is that FE simulation of micro-indentation requires a large amount of computing time even for one simulation. To determine the correct material parameter efficiently, the algorithm of the optimization technique to reduce the computing time is required.

In this thesis, we propose a novel method of material parameter identification using depth-sensing micro-indentation, FE simulation and optimization.

In Chapter 1, the previous research works on the micro-indentation are reviewed, especially focusing on material parameter identification using depth-sensing micro-indentation. Summarizing the problems in FE simulation based inverse approach to material parameter identification, the purpose and contents of this

thesis are put forward.

In Chapter 2, a framework of material parameter identification using depth-sensing micro-indentation, FE simulation and optimization is proposed. Details of micro-indentation experiments, FE models and scheme of material parameter identifications are described.

In Chapter 3, the details of an optimization technique named MARS [1] (multi-point approximation methodology based on response surface fitting), which was employed in the present work, are described. A special numerical technique to reduce computing time using the high- and low-fidelity interaction models is indicated.

In Chapter 4, viscoplasticity parameters of Sn-3.5Ag-0.75Cu lead-free solder alloy were identified using micro-indentation. Microscopically this alloy consists of different phases, mainly Sn-rich phase and Sn-Ag-Cu eutectic constituent, so that two different scale-sizes in material parameter identification were taken into account. One is the identification of *macro-scale properties* (or in other words, bulk properties) of the alloy, and the other is the *micro-scale properties* for individual phases.

In Chapter 5, a method for plasticity parameter identification of coating for coating/substrate systems is presented, which includes the guideline for selection of indenter type and an appropriate indenter-penetration depth for a given coating thickness. As examples, plasticity parameters of two coatings, Zn and Zn-Al placed on steel sheets, were identified.

In Chapter 6, the conclusions and some remarks in the present work are summarized.

References:

[1] M. V. Swain : Mat. Sci. Eng., A253 (1998) 160-166.

[2] K. Ohgushi, K. Homma, M. Ichikawa, N. Okabe, T. Takamatsu, T. Matsumura and Y. Abe : J. Jpn. Soc. Mech. Eng., A64 (1998) 681-688.

[3] Y. T. Cheng, C. M. Cheng : Surf. Coat. Technol., 133-134 (2000) 417-424.

[4] A. Nayebi, R. E. Abdi, O. Bartier and G. Mauvoisin : Mech. Mater., 34 (2002) 243-245.

[5] K. Tunvisut, N. P. O'Dowd and E. P. Busso : Int. J. Solids Struct., 38 (2001) 335-351.

[6] H. Hamasaki, F. Yoshida, K. Shinbata and V. V. Toropov : Proc 5th WCSMO, (2003) 101-102.

[7] H. Hamasaki, V. V. Toropov, K. Shinbata and F. Yoshida : J. JSTP, 46 (2005) 397-401 (in Japanese).

[8] H. Hamasaki, K. Shinbata and F. Yoshida : Mater. Trans.,

[9] F. Yoshida and H. Hamasaki :

[10] H. Hamasaki and F. Yoshida :

[11] I. J. McColm : Ceramic Hardness, Plenum, New York (1900).

[12] D. Tabor : Proc. R. Soc. Lond., A192 (1948) 247-274.

[13] D. Tabor : Hardness of Metals, Clarendon Press, Oxford (1951).

[14] R. Hill, B. Storåkers and A. B. Zdunek : Proc. R. Soc. Lond., A423 (1989) 301-330.

[15] B. Storåkers and P. L. Larsson : J. Mech. Phys. Solids., 42 (1994) 307-332.

[16] S. Timoshenko, J. N. Goodier : Theory of Elasticity, McGrawHill, New York (1951).

[17] S. L. Bulychev, V. P. Alekhin, M. K. Shorshorov. A. P. Ternovski and G. D. Shmyrev : Int. Lab., 41 (1975) 1409-1412.

[18] M. F. Doerner and W. D. Nix : J. Mater. Res., 1 (1986) 601-612.

[19] W. C. Oliver and G. M. Pharr : J. Mater. Res., 7 (1992) 1564-1571.

[20] G. M. Pharr : Mater. Sci. Eng., A253 (1998) 151-159.

[21] M. Göken and M. Kempf : Acta Metall., (1999) 1043-1052.

[22] D. J. Strange and A. K. Varshneya : J. Mater. Sci., 36 (2001) 1943-1949.

[23] J. S. Field and M. V. Swain : J. Mater. Res., 8 (1993) 297-306.

[24] J. S. Field and M. V. Swain : J. Mater. Res., 10 (1995) 101-112.

[25] J. S. Field and M. V. Carbon, 34 (1996) 1357-1366.

[26] E. Meyer : Z. Ver. Deutshe. Ing., 52 (1908) 645-654.

[27] H. O'Neill : Proc. Inst. Mech. Eng., 151 (1944) 116-130.

[28] J. R. Matthews : Acta Metall., 28 (1980) 311-318.

[29] A. L. Norbury and T. Samuel : J. Iron Steel. Inst. London, 117 (1928) 673-688.

[30] T. A. Adler : J. Am. Ceram. Soc., 77 (1994) 3177-3185.

[31] T. A. Adler and Ö. N. Doğan : Wear, 203-104 (1997) 257-266.

[32] S. Kucharski and Z. Mróz : Mater. Sci. Eng., A318 (2001) 65-76.

[33] S. Kucharski and Z. Mróz : J. Test. Eval., 31 (2003) 106-115.

[34] S. Kucharski and Z. Mróz : Mater. Sci. Eng., A379 (2004) 448-456.

[35] T. Ogawa, A. Miyamoto, K. Ohshimizu and T. Ohsawa : J. Soc. Mat. Sci., Japan, 49 (2000) 666-671 (in Japanese).

[36] A. Miyamoto, T. Ogawa and T. Ohsawa : J. Soc. Mat. Sci., Japan, 51 (2002) 445-450.

[37] M. Fujiwara and M. Otsuka : Mater. Sci. Eng., A319-321 (2001) 929-933.

[38] M. Fujiwara : J. JILM, 52 (2002) 282-290.

[39] P. M. Sargent and M. F. Ashby : Mater. Sci. Tech., 8 (1992) 594-601.

[40] X. Ma, F. Yoshida and K. Shinbata : J. Mater. Sci. Lett., 21 (2002) 1397-1399.

[41] X. Ma and F. Yoshida : Appl. Phys. Lett., 82 (2003) 188-190.

[42] X. Ma, F. Yoshida and K. Shinbata : Mater. Sci. Eng., A344 (2003) 296-299.

[43] R. Nowak, F. Yoshida, J. Morgiel and B. Major : J. Appl. Phys., 85 (1999) 841-852.

[44] R. Nowak, M. Pessa, M. Suganuma, M. Leszczynski and F. Yoshida : Appl. Phys. Lett., 75 (1999) 2070-2072.

[45] G. Yu, H. Ishikawa, T. Egawa, T. Soga, J. Watanabe, T. Jimbo and M. Umeno : J. Crys. Growth., (1998) 701-705).

[46] D. Lebouvier, P. Gilormini and E. Felder : J. Phys. D : Appl. Phys., 18 (1985) 199-210.

[47] D. Lebouvier. P. Gilormini and E. Felder : Thin Solid Films, 172 (1989) 227-239.

[48] Y. Sun, T. Bell and S. Zheng : Thin Solid Films, 258 (1995) 198-204.

[49] V. V. Toropov and E. van der Giessen : Proc. IUTAM symposium on OPTIMAL DESIGN WITH

ADVANCED MATERIALS, Report No. 983 (1992).

[50] F. Yoshida, M. Urabe and V. V. Toropov : Int. J. Mech. Sci., 40 (1998) 237-249.

[51] T. Nakamura, T. Wang and S. Sampath : Acta. Mater., 48 (2000) 4293-4306.

[52] Y. Gu, T. Nakamura, L. Prchlik, S. Sampath and J. Wallace : Mater. Sci. Eng., A345 (2003) 223-233.

[53] R. Rikards, A. Flores, F. Ania, V. Kushnevski and F. J. Baltá Calleja : Compt. Mater. Sci., 11 (1998) 233-244.

[54] A. Constantinescu and N. Tardieu : Proc. ISIP2000, (2000) 181-190.

Chapter 2: Framework of material parameter identification by depth-sensing micro-indentation experiments and FE simulation

As mentioned in Chapter 1, the micro-indentation test is not an experimental technique which determine directly stress-strain relationship of a material. Although some researches have suggested several methods to obtain the material parameters of plasticity [1-5] and creep [6-10], all of them need to use specific types of constitutive model, such as Ludwik-type plasticity and Norton-type creep law. Contrary to these, in this thesis, a framework of material parameter identification, which can use any types of constitutive models, based on the inverse approach is presented. Here, a set of material parameters are identified by minimizing the difference in *P-h* responses between FE simulation and the corresponding experimental result. The following items are presented in this Chapter:

- Micro-indentation experiment,
- FE model for micro-indentation,
- Method of material parameter identification,
- Application of this method and verification.

2.1 Micro-indentation experiment

2.1.1 Experimental apparatus

For micro-indentation, a depth-sensing micro-indenter MZT-4 (Akashi Co. Ltd.) was employed (see Fig. 2-1). During the loading process, the indenter is loaded with a constant loading speed until the load reaches to the maximum load, and subsequently it was unloaded in a certain time period after load-holding process. Indentation load (P) vs. indenter-penetration depth (h) curve is recorded during the indentation process. Three types of indenter, the Berkovich indenter (a pyramidal indenter of a triangular base and the angle between the vertical axis and its facet of 65°) and two spherical indenters (radii are 25 μm and 100 μm), were employed (See Fig 2-2 (a) and (b)). Since the shape of the Berkovich indenter is self-similar, it is not capable to observe the workhardening characteristics of a material so that spherical indenters were used for elastic-plastic workhardening materials. On the other hand, Berkovich indenter is appropriate for small materials, since its contact area is much smaller than that of the spherical indenters at a given indentation penetration.

2.1.2 Preparation of specimen

A rectangular block with a square surface of 10×10 mm was cut from a tested material, and embedded into a resin. Upper and bottom surfaces were parallelized to enable the indenter to sink vertically into the specimen surface. Due to the small indenter-penetration depth, prior to the experiments, surface of specimens were mechanically polished to make smooth surfaces and cleaned with acetone.

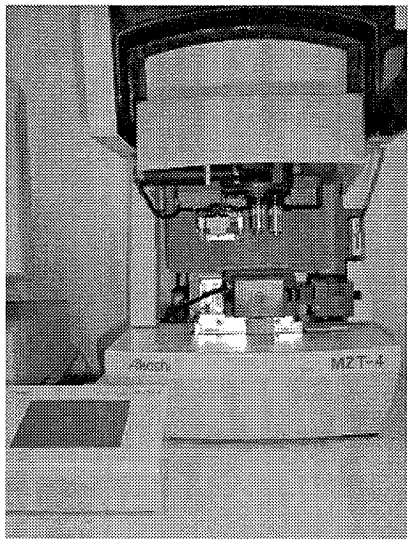

Fig. 2-1 Picture of depth-sensing micro-indenter MZT-4.

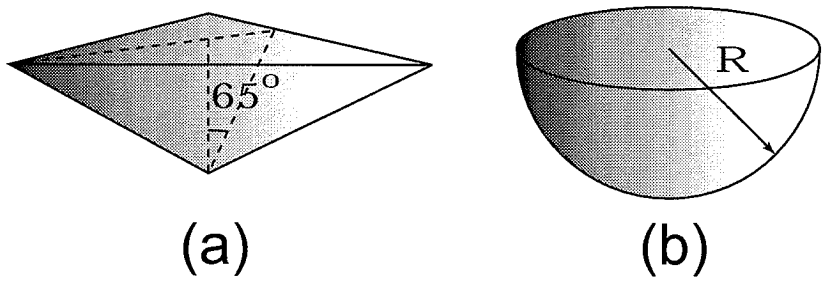

Fig. 2-2 Schematics of indenters; (a) Berkovich indenter; (b) spherical indenter.

2.2 Numerical simulation

For numerical simulation, a FE-code of MSC Marc-K7.3 was employed. Since three dimensional analysis requires tremendous computing time for solving elastio-plasticity contact problems, the model of micro-indentation was built with axisymmetric four-node-elements as an approximation, where the shape of the Berkovich indenter was approximated to the cone indenter. To build this cone-indenter approximation, we assumed that the Berkovich and its cone approximation indenters should have the same contact area for a given indentation penetration depth. (see Fig. 2-3) [11]. Contact areas for the Berkovich and cone indenter are calculated in Eq. (2-1) and Eq. (2-2) respectively:

$$S_B = \frac{3\sqrt{3}h_B^2 \sin\theta_B}{\cos^2\theta_B} \tag{2-1}$$

$$S_c = \frac{\pi h_c^2 \sin\theta_c}{\cos^2\theta_c} \tag{2-2}$$

where S, h and θ denote contact area, height and angle between the vertical axis and its facet, respectively, where subscripts B and c indicate the Berkovich and cone indenter, respectively. When contact areas of both indenters are the same (namely $S_B = S_c$, $h_B = h_c$), $\theta_c = 71°$ is calculated. Fig. 2-4 shows the FE model for the Berkovich indentation, and Fig. 2-5 shows two calculated P-h curves for an indentation test, one is a real three-dimensional analysis for Berkovich indenter and the other is axisymmetric approximation for cone indenter. By comparing these two curves, we confirmed that this axisymetric approximation is accurate enough for P-h calculation. Since indenters, which were used for micro-indentation experiments, were made from diamond, those were assumed as rigid material.

In FE simulation, the smaller number of elements, the shorter computing time. Therefore, several FE simulations with various smallest element size and size of entire model of material were performed and preferable FE model, which gives us P-h response with good accuracy in a realistic computing time, were determined for each micro-indentation simulation.

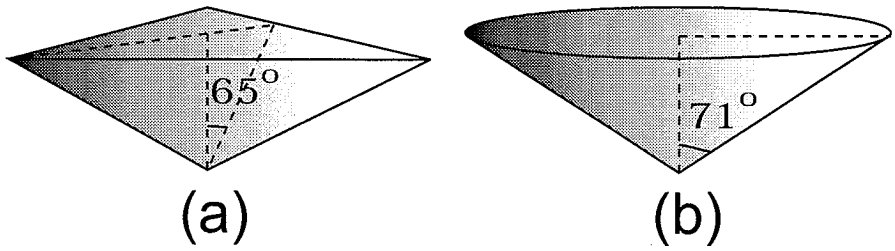

Fig. 2-3 Schematics of; (a) Berkovich indenter; (b) its cone approximation which has the same contact area to height ratio for axisymmetric FE model.

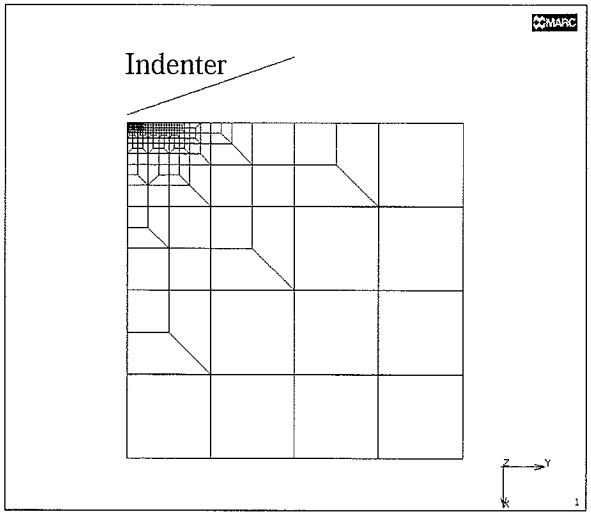

Fig. 2-4 Axisymmetric FE model for Berkovich indentation.

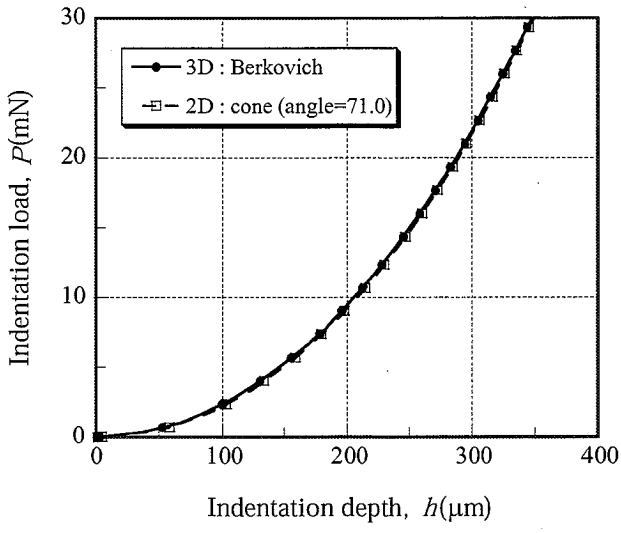

Fig. 2-5 Comparison of two calculated *P-h* curves for an indentation test, one is a real three-dimensional analysis for Berkovich indenter and the other is axisymmetric approximation for cone indenter.

2.3 Method of material parameter identification based on inverse approach

Fig. 2-6 shows the flowchart for material parameter identification using micro-indentation and FE simulation. From a micro-indentation test, a *P-h* curve is obtained. Then assuming a set of material parameters, such as yield strength and workhardening exponent, in a constitutive model, FE simulation of the indentation is carried out, and *P-h* response is obtained. By iteratively correcting the values of the parameters, appropriate values of the material parameters, with which the calculated *P-h* curve fits well to the corresponding experimental result, are determined. For this iterative process, some optimization techniques are necessary [12, 13]. In the present work, multipoint approximation methodology based on response surface fitting (MARS [14]) with the high- and low-fidelity interaction modeling is employed. The details of the optimization techniques are described in the next chapter.

2.4 Validation of the proposed method

For the validation of the proposed method, a spherical indentation was performed on a mild steel sheet and its plasticity parameters (yield strength Y, workhardening coefficient C and workhardening exponent n) in Ludwik type of constitutive model ($\sigma = Y + C(\varepsilon^p)^n$) were identified. Fig. 2-7 shows the experimental *P-h* curve and FE simulation result incorporating with the set of material parameters. Calculated *P-h* curve fits well to the experimental result and plasticity parameters were successfully determined as $Y = 200$ MPa, $C = 500$ MPa and $n = 0.55$. Fig. 2-8 is the corresponding stress-plastic strain curves between Ludwik type of constitutive model with thus identified parameters and uniaxial tension test result of the same material. Since these two curves also fit well with each other, the validation of the proposed method is confirmed.

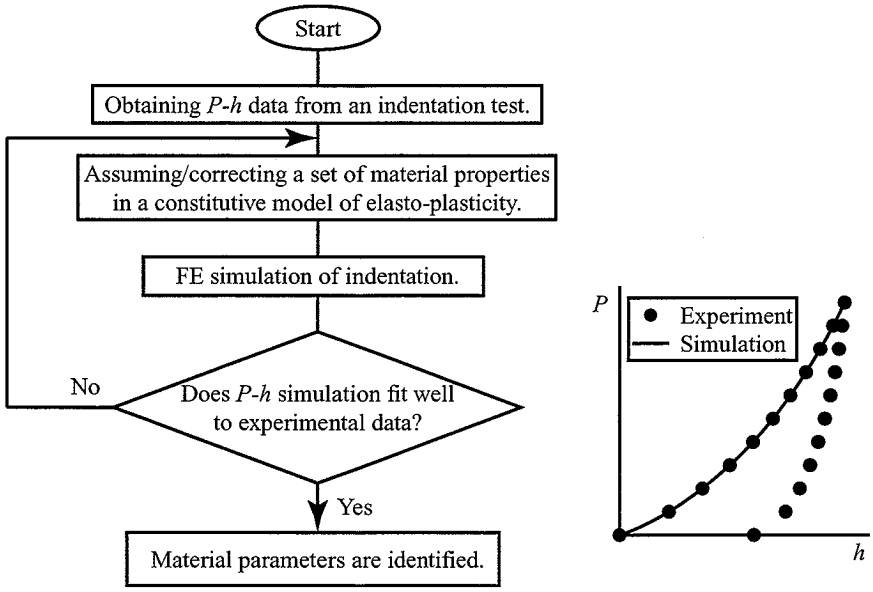

Fig. 2-6 Flowchart of material parameter identification based on inverse approach using micro-indentation experiment and FE simulation.

2.5 Conclusions

In this Chapter, the concept and the procedure of material parameter identification using depth-sensing micro-indentation, FE simulation and optimization have been presented. This technique has the following features:

1. An inverse approach, where FE simulation is iteratively performed by correcting a set of material parameter until its *P-h* curve fits well to the corresponding experimental result, is presented.
2. For material parameter identification, appropriate indenter type should be selected depending on material characteristics of a specimen. For example, Berkovich indentation, namely self-similar indentation, is not capable to identify workhardening parameter of plasticity so that the spherical indenter should be chosen in this case.
3. A two-dimensional axisymmetric model is employed for FE simulation. Since Berkovich indenter is a triangular shape, a three dimensional model is necessary. Therefore, this indenter is approximated by a cone indenter which has the same height to area ratio. By comparing *P-h* curve calculated from a real three-dimensional model with Berkovich indenter and its two-dimensional approximation, the validation of approximation is confirmed.
4. To perform the material parameter identification process systematically, an optimization technique is introduced. This optimization software automatically changes a set of material parameters in FE simulation iteratively and efficiently finds an optimal solution.
5. The validation of the proposed method is confirmed by applying it for a mild steel sheet. As a result, stress-strain curve, which is calculated by Ludwik type of constitutive model incorporating with the

identified material parameters, shows a good agreement with the uniaxial tension test result.

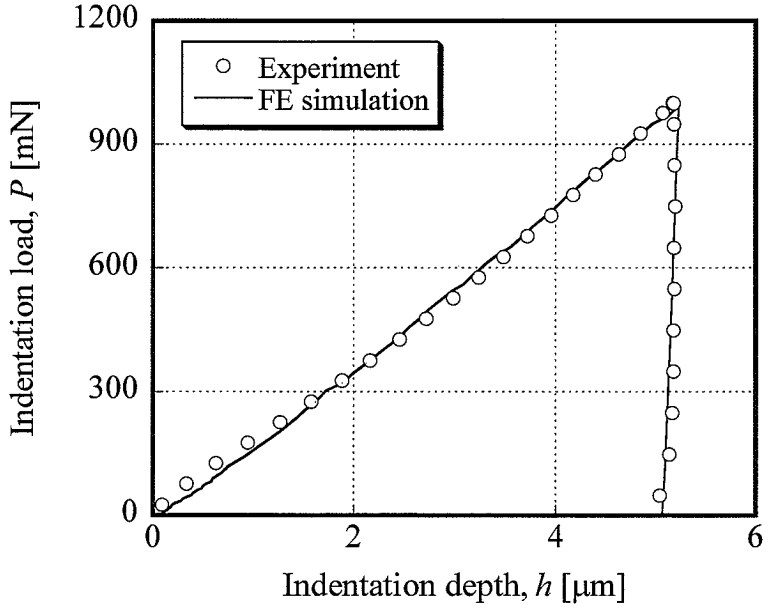

Fig. 2-7 Experimental *P-h* curve for mild steel and the corresponding FE simulation result incorporating with thus identified set of plasticity parameters of the Ludwik type of constitutive model.

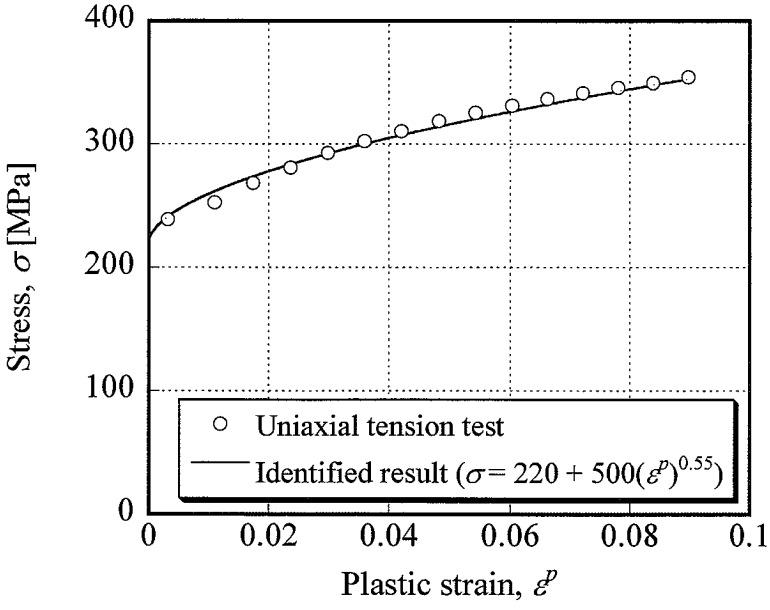

Fig. 2-8 Comparison of stress-strain curves between Ludwik type of constitutive model with the identified set of plasticity parameters and an uniaxial tension test result.

References

[1] T. A. Adler : J. Am. Ceram. Soc., 77 (1994) 3177-3185.

[2] T. A. Adler and Ö. N. Doğan : Wear, 203-104 (1997) 257-266.

[3] S. Kucharski and Z. Mróz : Mater. Sci. Eng., A318 (2001) 65-76.

[4] S. Kucharski and Z. Mróz : J. Test. Eval., 31 (2003) 106-115.

[5] S. Kucharski and Z. Mróz : Mater. Sci. Eng., A379 (2004) 448-456.

[6] T. Ogawa, A. Miyamoto, K. Ohshimizu and T. Ohsawa : J. Soc. Mat. Sci., Japan, 49 (2000) 666-671 (in Japanese).

[7] A. Miyamoto, T. Ogawa and T. Ohsawa : J. Soc. Mat. Sci., Japan, 51 (2002) 445-450.

[8] M. Fujiwara and M. Otsuka : Mater. Sci. Eng., A319-321 (2001) 929-933.

[9] M. Fujiwara : J. JILM, 52 (2002) 282-290.

[10] P. M. Sargent and M. F. Ashby : Mater. Sci. Tech., 8 (1992) 594-601.

[11] K. Kanazawa, H, Hirokawa and T. Yoshizawa : J. Jpn. Soc. Mech. Eng., A63 (1997) 567-576 (in Japanese).

[12] H. Hamasaki, F. Yoshida, K. Shinbata and V. V. Toropov : Proc 5th WCSMO, (2003) 101-102.

[13] H. Hamasaki, V. V. Toropov, K. Shinbata and F. Yoshida : J. JSTP, 46 (2005) 397-401 (in Japanese).

[14] V. V. Toropov : Struct. Optim., 1 (1989) 37-46.

Chapter 3: Optimization techniques for material parameter identification

In the recent work, material parameter identification is treated as an optimization problem. In this chapter, the detail of an optimization technique named MARS [1] (multi-point approximation methodology based on response surface fitting) is described. A special numerical technique to reduce computing time using the high- and low-fidelity interaction models is indicated.

3.1 Multi-point approximation methodology based on response surface fitting

A general optimization problem without constraint can be formulated as:

$$\begin{aligned} &F_0(\boldsymbol{x}) \rightarrow \text{minimize} \\ &A_i \le \boldsymbol{x}_i \le B_i \ \ (i=1,\ldots,N) \end{aligned} \tag{3-1}$$

where $F_0(\boldsymbol{x})$ is an objective function which is minimized during the optimization process and vector $\boldsymbol{x}$ is a set of design variables. A_i and B_i are the side constraint for each design variable and N is total number of design variables. The multipoint approximation method replaces the optimization problem by a sequence of approximate optimization problems:

$$\begin{aligned} &\tilde{F}_0^k(\boldsymbol{x}) \rightarrow \text{minimize} \\ &\tilde{A}_i^k \le x_i \le \tilde{B}_i^k \ , \ \tilde{A}_i^k \ge A_i \ , \ \tilde{B}_i^k \le B_i \ \ (i=1,\ldots,N) \end{aligned} \tag{3-2}$$

where k is the iteration number.

In each iteration, the approximate response functions $\tilde{F}_0^k(\boldsymbol{x})$ are intended to be adequate in a current search sub-domain. This is achieved by appropriate planning of numerical experiments and use of move limits defined by the side constrains $\tilde{A}_i^k$ and $\tilde{B}_i^k$. Moreover, it is attempted to achieve the best quality of the approximation functions in those regions of the design variable space, where the solution of the approximate optimization problem can be expected, *e.g.* on the boundary of the feasible region.

The approximation is determined by means of weighted least squares, which leads:

$$G_k(\boldsymbol{a}) = \sum_{p=1}^{P} w_p^k \left[F_0(\boldsymbol{x}_p) - \tilde{F}_0^k(\boldsymbol{x}_p, \boldsymbol{a}^k) \right]^2 \rightarrow \text{minimize} \tag{3-3}$$

Here minimization is carried out with respect to the tuning parameters $\boldsymbol{a}^k$, where w_p^k refers to the weight coefficient and p, $(p=1,\ldots,P)$ is the number of experimental point. Fig. 3-1 shows the schematic of the idea of MARS for design variables $N=2$.

Let us now consider the problem of selection of the structure of the simplified expressions $\tilde{F}_0(\boldsymbol{x},\boldsymbol{a})$. The efficiency of the optimization technique depends greatly on their accuracy. Note that properly chosen simplified expressions in our case of the optimization problem with no behavioural constraints imposed, must allow for internal minimum point inside the search region defined by side constraints A_i and B_i. Otherwise, the convergence of the method can be slow; i.e. the number of calls for the evaluation of the functions $F(\boldsymbol{x}_p)$ would be large. The simplest form of an expression which satisfies the above

requirement, is a full quadratic polynomial in $\boldsymbol{x}$ (linear in $\boldsymbol{a}$):

$$\tilde{F}(\boldsymbol{x},\boldsymbol{a}) = a_0 + \sum_{i=1}^{N} a_i x_i + \sum_{i\le j}^{N} a_{ij} x_i x_j \tag{3-4}$$

which contains (N+1)(N+2)/2 tuning parameters to be found in each iteration by the least-squares surface fitting.

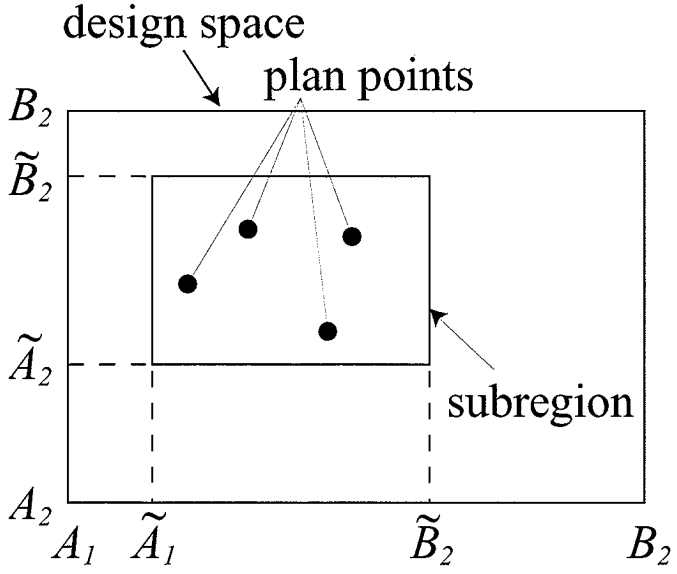

Fig. 3-1 Illustration of the idea of MARS

3.2 Material parameter identification problem for optimization

Let us consider the material parameters to be identified as components of the vector $\boldsymbol{x} \in \boldsymbol{R}^N$. Then the inverse problem can be formulated as a following optimization problem [2]:

Find the vector $\boldsymbol{x}$ that minimizes the objective function

$$F_0(\boldsymbol{x}) = \sum_{\alpha=1}^{L} \Theta^\alpha F^\alpha(\boldsymbol{x}) \tag{3-5}$$

$$F^\alpha(\boldsymbol{x}) = \frac{\sum_{s=1}^{S_\alpha} \left(h_s^\alpha - h^\alpha(\boldsymbol{x}, P_s^\alpha)\right)^2}{\sum_{s=1}^{S_\alpha} \left(h_s^\alpha\right)^2} \tag{3-6}$$

where L is the total number of individual specific response quantities (denoted by α) which can be measured in the course of micro-indentation experiments and then obtained as a result of the numerical simulation. In this thesis, the following notations are used:

$P_s^\alpha : (\alpha = 1,\ldots,L,\ s = 1,\ldots,S)$: the discrete set of S_α data points, corresponding to the discrete values of the load,

h_s^α : the value of the α-th measured indentation penetration depth corresponding to the value of the experiment history parameter (load P_s^α),

$h^\alpha\left(\boldsymbol{x}, P_s^\alpha\right)$: the value of the same response quantity (indenter-penetration depth) obtained from the FE simulation,

Θ^α : the weight coefficient which determines the relative contribution of information yielded by α-th set of experimental data.

The optimization problem has the following features:

1. the objective function is an implicit function of parameters $\boldsymbol{x}$,
2. to calculate values of this function for the specific set of parameters $\boldsymbol{x}$ means to use a nonlinear numerical (*e.g.* finite element) simulation, which involves a large amount of computation time,
3. function values may present some level of numerical noise, i.e. can only be estimated with the finite accuracy.

Fig. 3-2 shows an illustration of the idea of experimental and simulated response quantities h^α corresponding to various values of the experiment history parameter $P_s^\alpha:\left(\alpha=1,\ldots,L,\ s=1,\ldots,S\right)$.

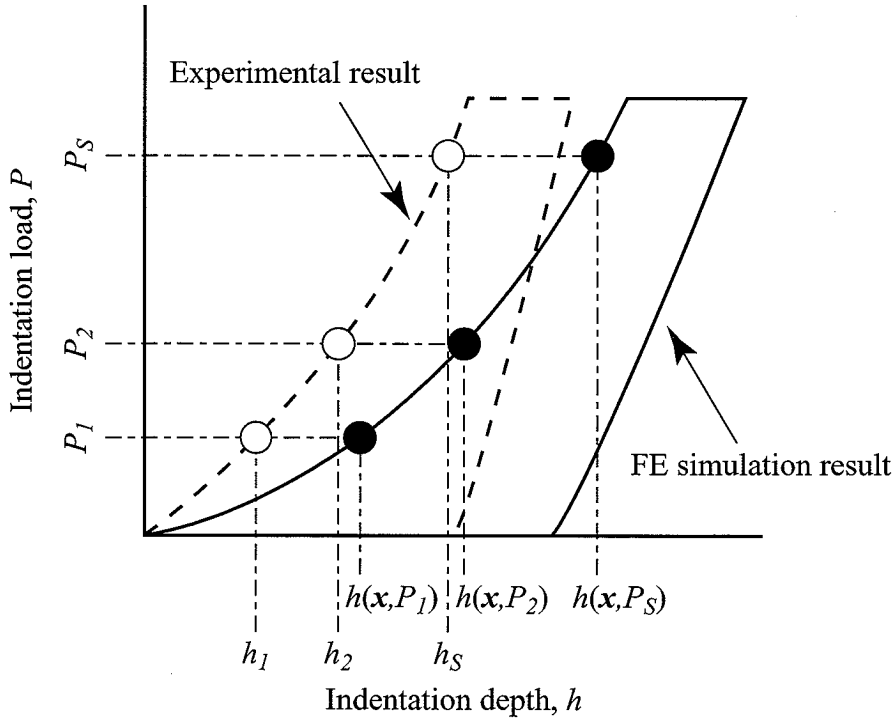

Fig. 3-2 The response quantity h^α at various values of the history parameter $P_s^\alpha:\left(s=1,\ldots,S\right)$ as obtained from the experiment (○), and form numerical simulations (●).

3.3 Optimization problem using the interaction of high- and low-fidelity models

3.3.1 Optimization based on the interaction of high- and low-fidelity model

An iterative numerical optimization procedure for the material parameters identification needs a large

number of high-fidelity process simulations (*e.g.* finite element analysis using fine mesh) to obtain accurate responses of the objective function $F_0(\boldsymbol{x})$. The serious problem for such a high-fidelity model simulation is a large amount of required computing time. Therefore, a low-fidelity process simulation using a simplified numerical model in conjunction with approximation functions [3] is introduced to reduce the number of the high-fidelity simulations and shorten the computing time considerably with keeping the accuracy of the response corresponding to the high-fidelity simulations. For example, the finite element analysis using a coarse mesh or an analysis using simplified mechanistic model can be utilized as a low-fidelity simulation. Such a low-fidelity model should inherit important features of the original high-fidelity model, be less computationally expensive and provide a good basis for development of high quality approximation.

The following approximation function $\tilde{f}_0(\boldsymbol{x},\boldsymbol{b})$ have been used instead of the original ones $F_0(\boldsymbol{x})$ for the iterative response analysis in the optimization procedure:

$$\tilde{f}_0(\boldsymbol{x},\boldsymbol{b}) \equiv \tilde{f}_0(f(\boldsymbol{x}),\boldsymbol{b}) \tag{3-7}$$

where $f(\boldsymbol{x})$ is the response of objective function using the low-fidelity simulation and the vector $\boldsymbol{b}$ consists of tuning parameters to correct the low-fidelity response. The approximated function reflects the main properties of the original high-fidelity model and it is computationally less expensive. Depending on the problem, several types of the approximation functions can be employed. Alternatively, the tuning parameters can be introduced in an explicit correction function $R(\boldsymbol{x},\boldsymbol{b})$, which also depends on the design variables. In this paper, the approximation using linear model with full cubic polynomial was employed.

$$\tilde{f}_0(\boldsymbol{x},\boldsymbol{b}) = f(\boldsymbol{x}) + R(\boldsymbol{x},\boldsymbol{b}) \tag{3-8}$$

$$R(\boldsymbol{x},\boldsymbol{b}) = b_0 + \sum_{i=1}^{N} b_i x_i + \sum_{i\le j}^{N} b_{ij} x_i x_j + \sum_{j\le k}^{N} b_{ijk} x_i x_j x_k \tag{3-9}$$

where N is number of design variables $\boldsymbol{x}$. The set of tuning parameters $\boldsymbol{b}$ are to be determined by least squares surface fitting using the original function values at several points of the design variable space.

3.3.2 Choice of design of experiments

The choice of the design of experiments can have a large influence on the accuracy of the correction function $R(\boldsymbol{x},\boldsymbol{b})$. In this work, the approach by Audze and Eglais [4] and later used by Rikards [5] is adopted. It considers a non-traditional criterion for elaboration of plans of experiments which is not dependent on the mathematical model of the object or process under consideration. The input data for the elaboration of the plan only include the number of factors N (number of design variable) and the number of experiments P. The main principles in this approach are as follows:

1. the number of levels of factors (same for each factor) is equal to the number of experiments and for

each level there is only one experiment;

2. the points of experiments are distributed as uniformly as possible in the domain of variables. There is a physical analogy with the minimum of potential energy of repulsive farces for a set of points of unit mass, if the magnitude of these repulsive forces is inversely proportional to the distance squared between points:

$$\sum_{p=1}^{P}\sum_{q=p+1}^{P}\frac{1}{L_{pq}^{2}} \rightarrow \text{minimize} \tag{3-10}$$

Here L_{pq} is the distance between the points having numbers p and q.

The design of experiments (DoE) is characterized by a matrix which contains the levels of factors for each of P experiments. In this work, the 10 point DoE was used. For a number of factors (design variables) N = 2, and the number of points P = 10, the matrix is described as follows;

8	10	4	6	2	3	9	5	7	1
1	7	10	6	8	5	4	2	9	3

The corresponding plan of experiments is shown in Fig. 3-3.

An example of deviations of the objective function values obtained by the low- and corrected low-fidelity model from the objective function value obtained by the high-fidelity model at 15 points within the variable space are shown in Fig. 3-4. First 10 points were used to build the correction function and the latter 5, which were not included in the first 10 points, were obtained for the validation. The blank bars correspond to the low-fidelity model and the black ones for corrected low-fidelity model. It can be seen that the correction function significantly improved the quality of the low-fidelity model. As a result, corrected low-fidelity model, which is computationally less expensive, could be used as an accurate approximation instead of the high-fidelity model, which is much time consuming during the optimization process. This allows significantly reduce the computing time of the whole optimization process.

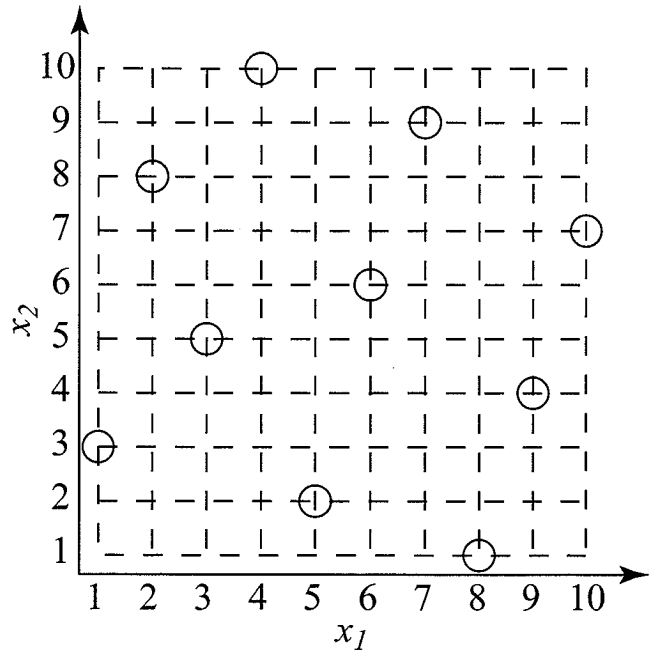

Fig. 3-3 Plan of experiments ($N = 2$, $P = 10$).

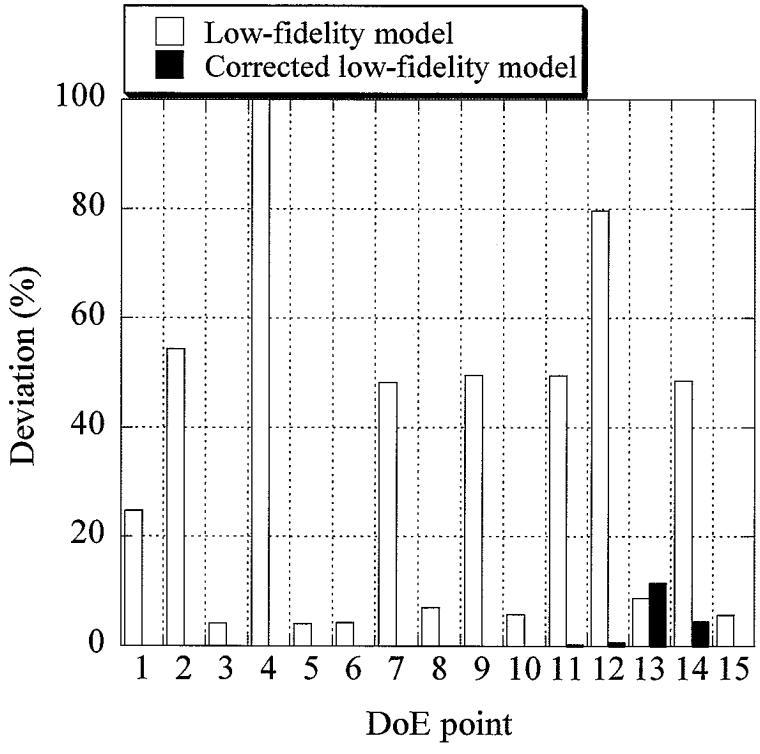

Fig. 3-4 Deviation of objective function values obtained by FE simulation using low- and corrected low-fidelity model from the corresponding value obtained by FE simulation using high-fidelity model at 15 points in the variable space.

3.4 Conclusions

In this chapter, details of optimization technique employed for an inverse approach are described. Significant features of this methodology is as follows:

1. Multi-point approximation methodology based on response surface fitting (MARS) is adopted to calculate the optimal solution. This technique allows us to reduce the whole computing time to solve the optimization problem, since FE simulation is performed only for building an approximation function of the objective function.

2. The squared deviation of *P-h* curve calculated by FE simulation from the corresponding experimental result is employed as the objective function to minimize the difference of these curves. When both two *P-h* curves are completely the same, objective function value will be zero, while this value increases as difference of two curves increases.

3. Even though MARS requires less number of FE simulations than conventional optimization technique, FE simulation itself needs a large amount of time even for a single simulation. Therefore, only low-fidelity FE model, which means a model consists of coarser mesh, is used during optimization process. To keep the accuracy corresponding to the high-fidelity model, the objective function value obtained from the result of low-fidelity model is corrected by the simple equation which is build from the numerical experiments to interacts the low- and high-fidelity models. The computing time for the material parameter identification process is dramatically reduced by adopting this method.

References

[1] V. V. Toropov : Struct. Optim., 1 (1989) 37-46.

[2] V. V. Toropov and E. van der Giessen : Proc. IUTAM symposium on OPTIMAL DESIGN WITH ADVANCED MATERIALS, Report No. 983 (1992).

[3] V. V. Toropov : In: Blachut, J.; Eschenauer, H. A. (eds.), Emerging Methods for Multidisciplicary Optimization, CISM Courses and Lectures, No. 425, Int. Centre Mech. Sci., (2001) 205-256.

[4] P. Audze and V. Eglais : New approach for planning out of experiments, Problems of Dynamics and Strengths, 35, Riga, Zinatne Publishing House, (1977) 104-107.

[5] R. Rikards : Proc IUTAM symposium, (1993) 149-162.

Chapter 4: Identification of viscoplasticity parameters of lead-free solder alloy

Since lead in Sn-Pb eutectic solder is harmful to human body, the development of lead-free solders, together with their joining technologies, has been greatly concerned. For an appropriate selection of a solder alloy and the designing of solder joints, it is essential to know those viscoplastic properties (or creep properties) since most of inelastic deformations of solder alloys are due to viscoplasticity rather than rate-independent plasticity. If we want to determine the properties of a solder in a joint of IC package on a print circuit board, for example, conventional material tests, such as uniaxial tension, will be hardly applicable because the volume of solder is too small. For such a case, the depth-sensing micro-indentation test has a great advantage over other conventional experimental techniques [1-5].

In this Chapter, viscoplasticity parameters of Sn-3.5Ag-0.75Cu lead-free solder alloy were identified using micro-indentation. Microscopically this alloy consists of different phases, mainly Sn-rich phase and Sn-Ag-Cu eutectic constituent (see Fig. 4-1), so that we have to think about two different scale-sizes in material parameter identification. One is the identification of *macro-scale properties* (or in other words, bulk properties) of the alloy, and the other is the *micro-scale properties* for individual phases. In the first part of this Chapter the bulk properties of the lead-free solder alloy is dealt with, and in the second part the viscoplasticity properties of the individual phases of the alloy are discussed.

4.1 Identification of bulk properties

4.1.1 Experiment

Sn-3.5Ag-0.75Cu lead-free solder alloy (Senjyu Co., Ltd.), which is expected as a standard lead-free solder alloy in next generation because of its high performances of, stability and reliability, was selected as a specimen. In this experiment, the Berkovich indenter and spherical indenter with the radius of 100 μm were employed. Maximum load of 500 mN for the Berkovich indentation and 700 mN for spherical indentation were selected, under which the scattering of *P-h* curves obtained from several indentation trials were very small. To determine rate-dependent material properties (viscoplasticity), two different loading speeds (100 $mN \cdot s^{-1}$ [fast] and 1 $mN \cdot s^{-1}$ [slow]) were selected, and moreover, the indentation creep (strain vs. time) at maximum-load holding for 5 seconds was recorded. The experimental conditions are summarized in Table 4-1.

4.1.2 Experimental results

Figs 4-2 and 4-3 show the *P-h* curves obtained from Berkovich and spherical indentations, respectively. It is obvious that the shapes of *P-h* curves were strongly depending on the types of indenters. *P-h* curves for the Berkovich indentation can be expressed by the power law relationship ($P = Kh^m$, where K and m are constants), while those for the spherical indentation are almost linear.

It should be noted that *P-h* responses are highly rate-dependent. The low loading speed gave deeper penetration depth. The indentation creep, *i.e.*, the increase of the indenter-penetration depth during the holding time, was observed in the fast loading, while in the slow loading almost no creep appeared.

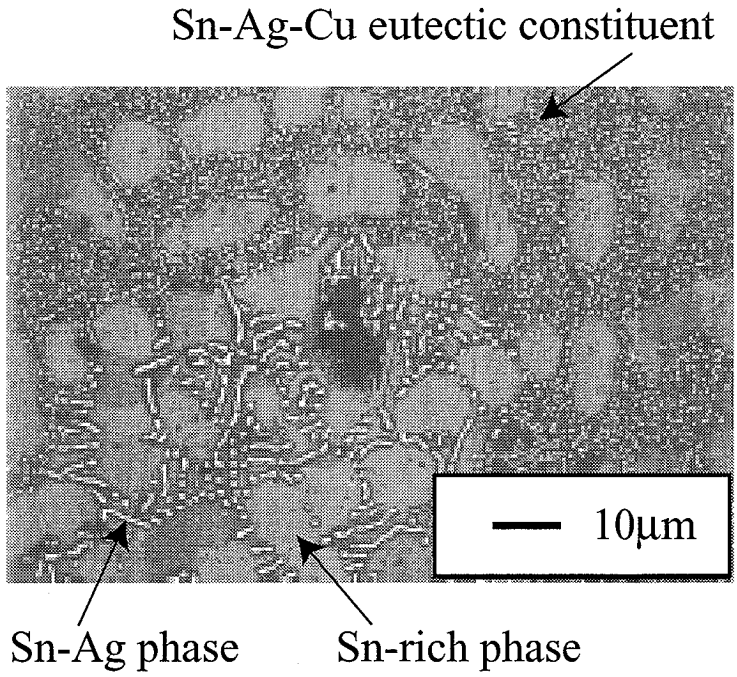

Fig. 4-1 SEM image of the surface of the Sn-3.5Ag-0.75Cu lead-free solder.

Table 4-1 Conditions of experiments for bulk Sn-3.5Ag-0.75Cu lead-free solder alloy.

Indenter	Maximum load [mN]	Loading speed [mN/s]	Holding time [s]
Berkovich	500	1.100	5
Spherical	700		

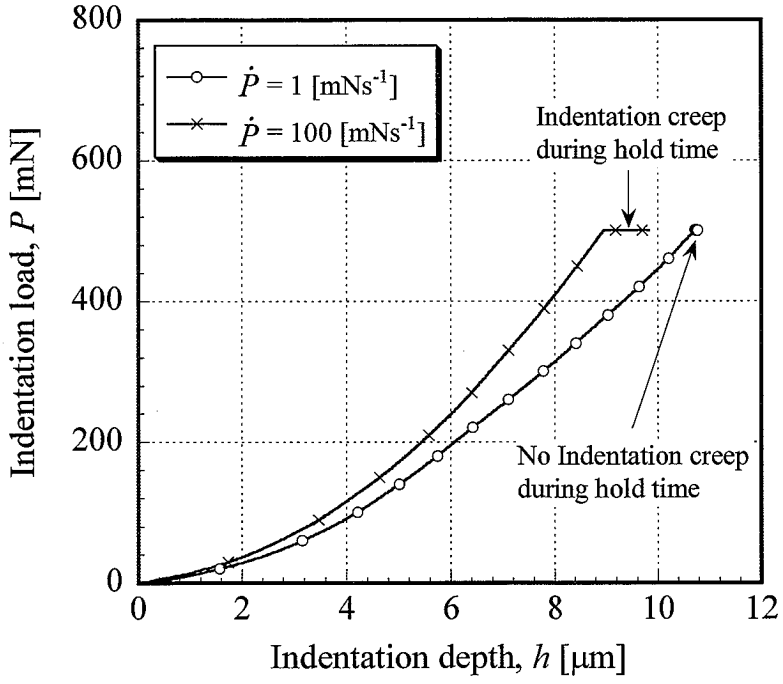

Fig. 4-2 Experimental *P-h* curves for Sn-3.5Ag-0.75Cu lead-free solder obtained from Berkovich micro-indentation.

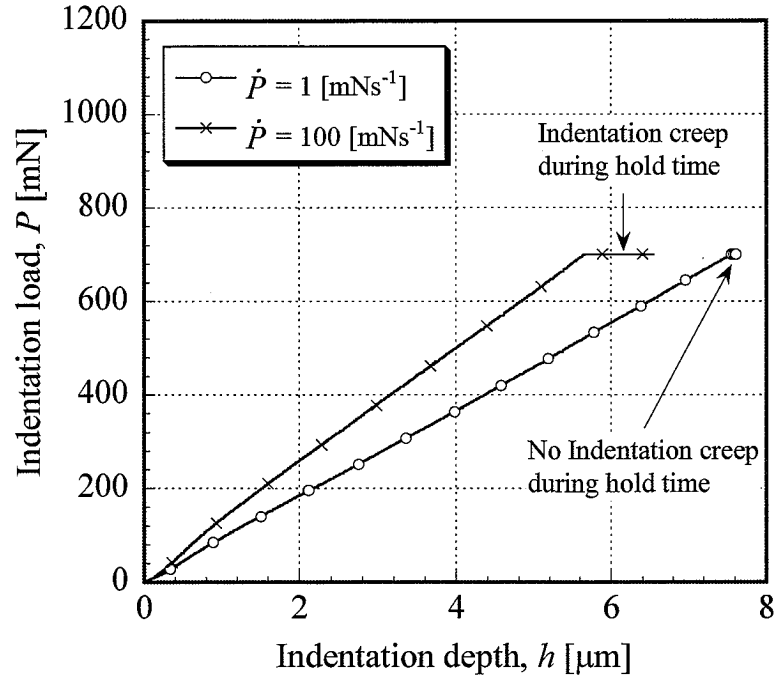

Fig. 4-3 Experimental *P-h* curves for Sn-3.5Ag-0.75Cu lead-free solder obtained from spherical micro-indentation.

4.1.3 Viscoplastic parameter identification

The lead-free solder shows strong rate dependency, while it has almost no workhardening except at small strain region. Hence, in this thesis, Norton's law expressed by Eq. (4-1) is assumed for its constitutive model:

$$\dot{\bar{\varepsilon}} = C\left(\frac{\bar{\sigma}}{\sigma_0}\right)^n, \tag{4-1}$$

where $\dot{\bar{\varepsilon}}$ and $\bar{\sigma}$ denote the equivalent viscoplastic strain rate and the equivalent stress, respectively. For the simplicity, the normalizing stress parameter σ_0 is assumed to be 1 MPa. C and n are material parameters to be identified. Young's modulus E = 35 GPa and Poisson's ratio ν = 0.3 were determined from uniaxial tension tests, since, for solder alloys, the deformation under micro-indentation is mainly viscoplastic and it is hardly possible to determine the elastic properties from *P-h* curves.

4.1.4 Results and discussions

The obtained material parameters were $C = 8.24\times10^{-23}$ and n = 11.3. Figs. 4-4 and 4-5 show experimental *P-h* curves and the corresponding FE simulation results incorporating with the identified set of material parameters for the Berkovich indentation and the spherical indentation, respectively. *P-h* curves obtained from FE simulations show a good agreement with the corresponding curves of micro-indentation experiment. In these figures, FE simulations well reproduce the rate-dependent *P-h* responses at loading and holding parts.

To validate thus identified material parameters, a bulk compression experiment of the same material (a cylindrical specimen with the diameter of 6 mm and height of 10 mm) was performed. In Fig. 4-6, the strain rate vs. stress relation given by the Eq. (4-1) incorporating the identified set of material parameter was compared with the bulk compression test result. From this figure, it is confirmed that the material parameters obtained from the micro-indentations experiment/simulation agree well with those determined from the bulk compression experiment.

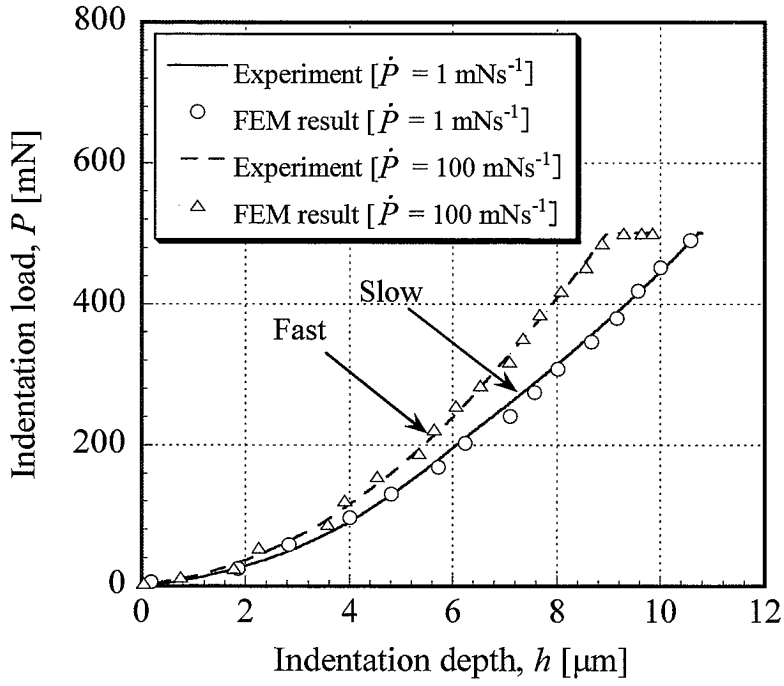

Fig. 4-4 Experimental *P-h* curves for Sn-3.5Ag-0.75Cu lead-free solder and the corresponding results of FE simulation incorporating the identified set of material parameters for Berkovich indentation.

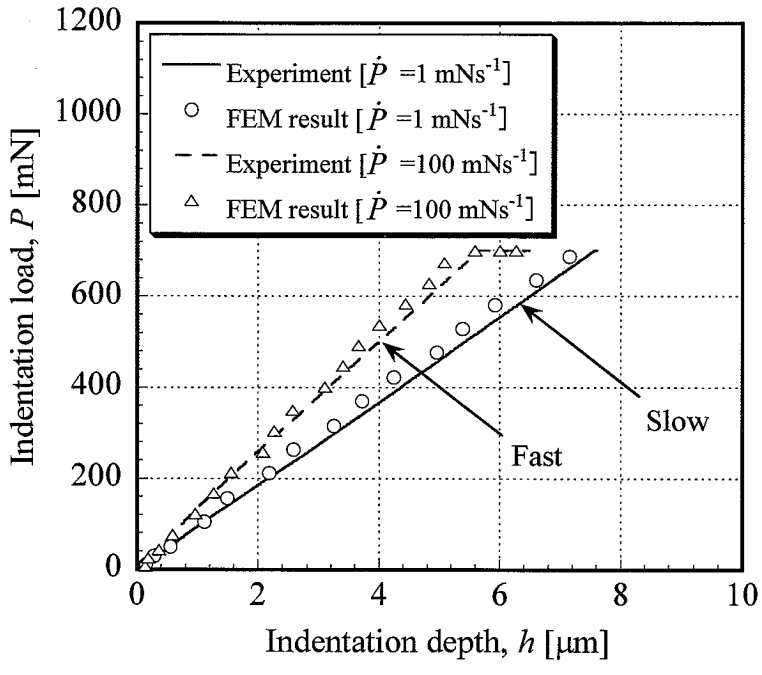

Fig. 4-5 Experimental *P-h* curves for Sn-3.5Ag-0.75Cu lead-free solder and the corresponding results of FE simulation incorporating the identified set of material parameters for spherical indentation.

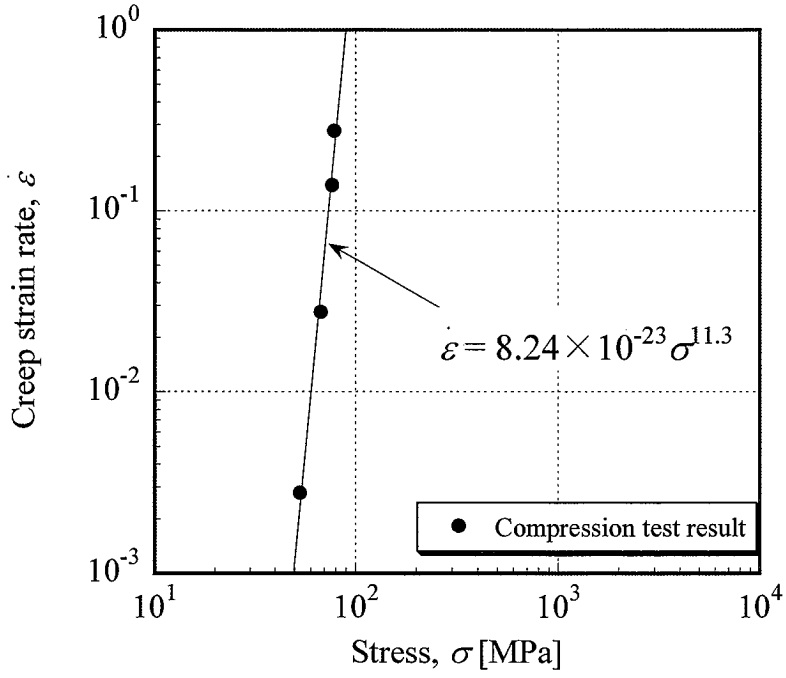

Fig. 4-6 Comparison of experimental data of stress vs. plastic strain rate under uniaxial compression with predicted result by Norton-type constitutive equation incorporating identified material parameters from micro-indentation.

4.1.5 Discussion of identification of viscoplasticity parameters from micro-indentation with self-similar indenters

Let us assume that the equivalent viscoplastic strain rate is given as a unique function of the equivalent stress. The deformation under micro-indentation is mostly viscoplastic, hence, for self-similar indentation such as the Berkovich indentation, the equivalent viscoplastic strain rate $\dot{\bar{\varepsilon}}$ at a certain point in a material is proportional to the normalized indentation penetration velocity $\dot{h}/h$. Namely,

$$\dot{\bar{\varepsilon}} = k_1 \left(\frac{\dot{h}}{h} \right), \tag{4-2}$$

where k_1 is a constant depending on the position of the material element. Since distribution of strain rate is depending on power law exponent n in Eq. (4-1), k_1 depends also on n. On the other hand, indentation load P is proportional to the equivalent stress $\bar{\sigma}$ and contact area between indenter and a material A. If we ignore the pile-up and sink-in during the indentation, A is almost proportional to h^2, so that;

$$P \approx k_2 \bar{\sigma} h^2 \tag{4-3}$$

where k_2 is a constant depending of the position the material element and power law exponent n. Provided that the equivalent stress $\bar{\sigma}$ keeps almost constant value under the constant loading speed $\dot{P}$, the

following relationship can be obtained:

$$\dot{P} \approx 2k_2 \bar{\sigma} \dot{h} h \tag{4-4}$$

From Eq. (4-1) and (4-2), indenter-penetration velocity is given by the equation:

$$\dot{h} = \frac{Ch}{k_1}\left(\frac{\bar{\sigma}}{\sigma_0}\right)^n \tag{4-5}$$

From Eqs. (4-3), (4-4) and (4-5), we finally obtain the following relationship:

$$P \approx \alpha \sigma_0^{n/n+1} C^{-1/n+1} \dot{P}^{1/n+1} h^{2n/n+1} \tag{4-6}$$

where $\alpha = \left(k_1 k_2^n / 2\right)^{1/n+1}$ is a non-dimensional value. This equation is useful to determine the viscoplasticity parameters. If two *P*-*h* responses $P_{(1)}$-$h_{(1)}$ and $P_{(2)}$-$h_{(2)}$ for different loading speed $\dot{P}_{(1)}$ and $\dot{P}_{(2)}$ are obtained, the power law exponent n can be easily calculated. Using indentation loads, $P_{(1)}$ and $P_{(2)}$, at the same penetration depth ($h_{(1)} = h_{(2)}$), the following relationship is obtained from Eq. (4-6).

$$n = \frac{\log\left(\dot{P}_{(2)} / \dot{P}_{(1)}\right)}{\log\left(P_{(2)} / P_{(1)}\right)} - 1 \tag{4-7}$$

If α is determined, constant C will be calculated from Eq. (4-6). Thus calculated n value for Sn-3.5Ag-0.75Cu lead-free solder alloy is 15.2, which is a bit larger than the value of n = 11.3 identified from inverse approach. Such a discrepancy would come from the fact that Eq. (4-6) includes some rough approximations and uncertain assumptions. Despite rough approximation of determined material parameters, this simplified dimensional analysis might be useful to determine the first estimation of material parameters for the FE simulation-based inverse approach, since FE simulation of micro-indentation for viscoplastic material needs large amount of computing time.

4.2 Identification of viscoplastic parameters for individual phases

As already mentioned, Sn-3.5Ag-0.75Cu lead-free solder is mainly consists of Sn-rich phase and Sn-Ag-Cu eutectic constituent. Since the volume of a solder alloy at the joined part is very small, the reliability of the solder joint would strongly depend on the heterogeneous stress existing in individual phases of the alloy. To calculate such a micro-scale stress distribution, it is necessary to know mechanical properties of the individual phases. For that purpose, in the present work, micro-indentation tests were performed on individual phases of Sn-3.5Ag-0.75Cu lead-free solder.

4.2.1 Guideline for indenter-penetration depth

In order to identify mechanical properties of a selected phase exclusively in a multi-phase material by micro-indentation, it is of vital importance to determine an appropriate indenter-penetration depth, because

if the indentation is too deep, *P-h* response will include the effect of deformation of the other neighboring phases. In order to determine a guideline for the indentation depth, FE simulation of micro-indentation was performed. Axisymmetric models for a homogeneous material and a dual-phase material are shematically illustrated in Figs(4-7) (a) and (b), respectively, where Phase 1 is for indentation and Phase 2 is its surrounding. The radius of Phases 1 and 2 were given as a = 3.4 μm and b = 30 μm, respectively. For the present numerical experiment, three materials, named Material 1, 2 and 3, which have different viscoplastic properties but has unique elastic properties (E = 50 GP and ν = 0.3), as listed in Table (4-2), were used. The relationship between viscoplastic strain rate and applied stress for these three materials are shown in Fig. (4-8). The properties of Material 1 correspond to those of bulk of Sn-3.5Ag-0.75Cu lead-free solder. Material 2 and 3 were assumed so as to be softer and harder than Material 1, respectively. Several combinations of materials were chosen for dual-phase material models. Here, the indentation is conducted always on Phase 1. To check how strongly the deformation of the surrounding phase (*i.e.*, Phase 2) influences the results of indentation, the difference in *P-h* responses between a dual phase (Phases 1+2) material and the corresponding homogeneous (Phase 1 only) material were numerically examined by FE simulation. The calculated results of *P-h/a* curves are summarized in Fig. (4-9), where (a), (b) and (c) are cases when materials 1, 2 and 3 are chosen for indented material (Phase 1), respectively. At the beginning of the indentwr-penetration, *P-h/a* curves of homogeneous and dual-phase model were tracing the same course and start to deviate at a certain indentation depth. To determine this deviation point quantitatively, the following measure of deviation is defined.

$$Deviation = \frac{|P_h - P_d|}{P_h} \tag{4-8}$$

where P_h and P_d denote the indentation load for homogeneous and dual-phase models for a given indenter-penetration depth, respectively. If we allow 2% deviation, for example, it is at $h/a \approx 0.15$ for all the cases (See Fig. (4-9), arrows indicate thus defined deviation points).

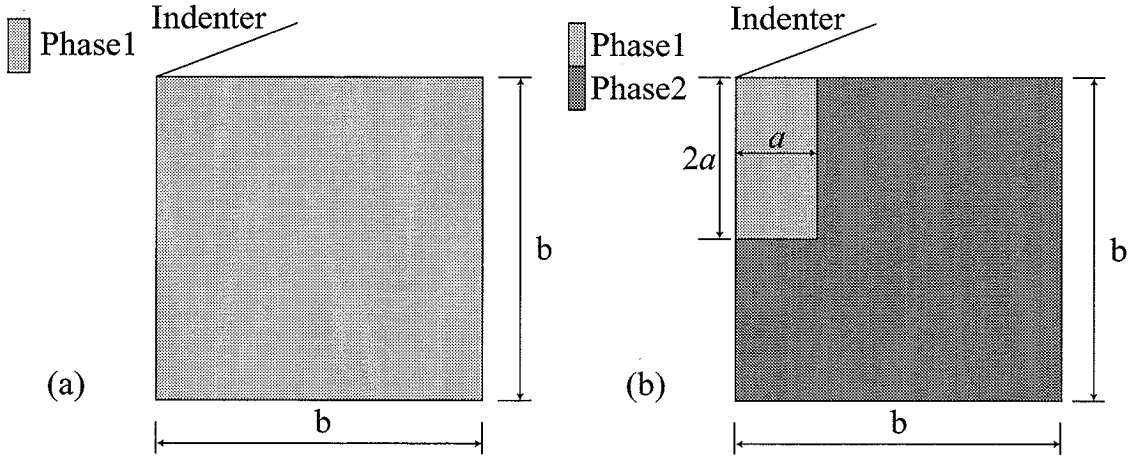

Fig. 4-7 Axisymmetric FE model with conical indenter for; (a) homogeneous material and; (b) dual-phase material.

Table 4-2 Material parameters for FE simulation.

	C	n	Young's modulus, E [GPa]	Poisson's ratio, ν
Material 1	8.39×10^{-23}	11.3		
Material 2	1.00×10^{-16}	10.0	50	0.3
Material 3	1.00×10^{-23}	10.0		

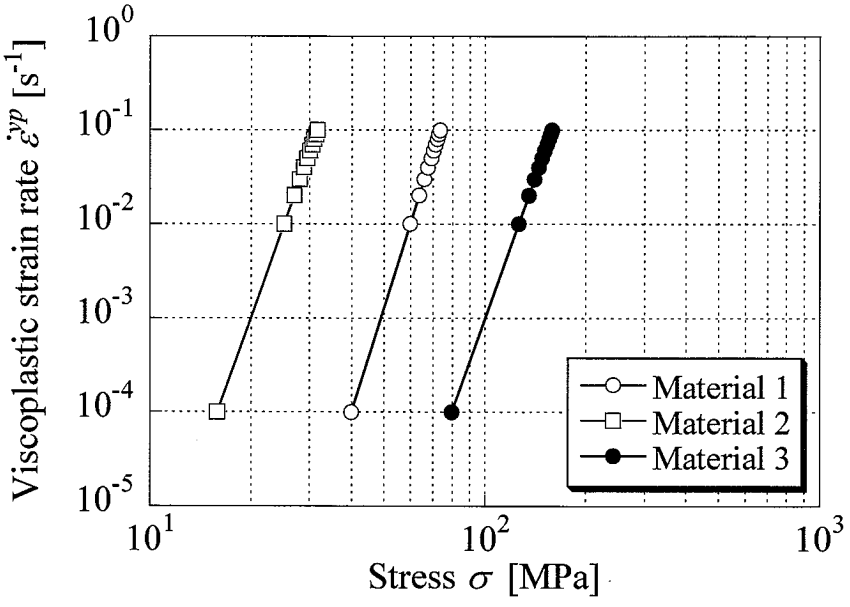

Fig. 4-8 Viscoplastic strain rate vs. stress relationships for Material 1, 2 and 3.

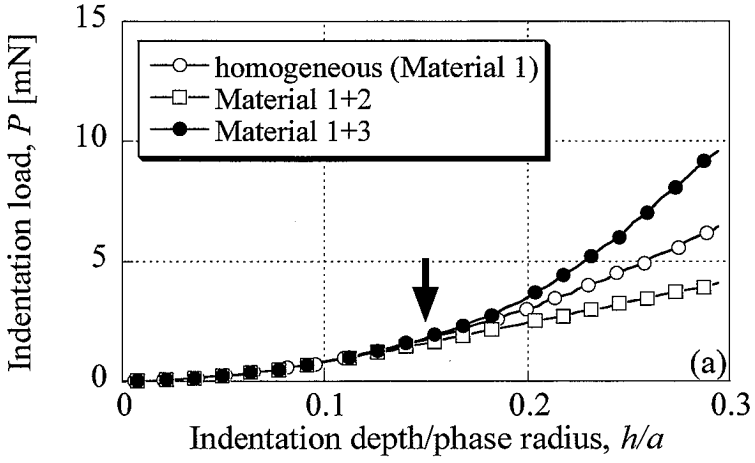

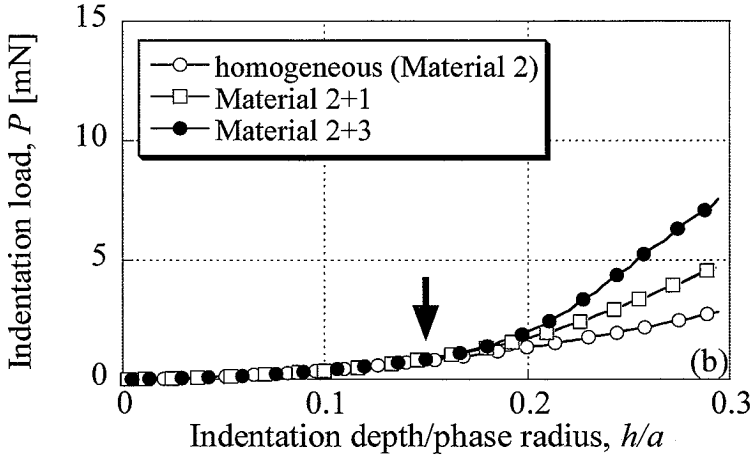

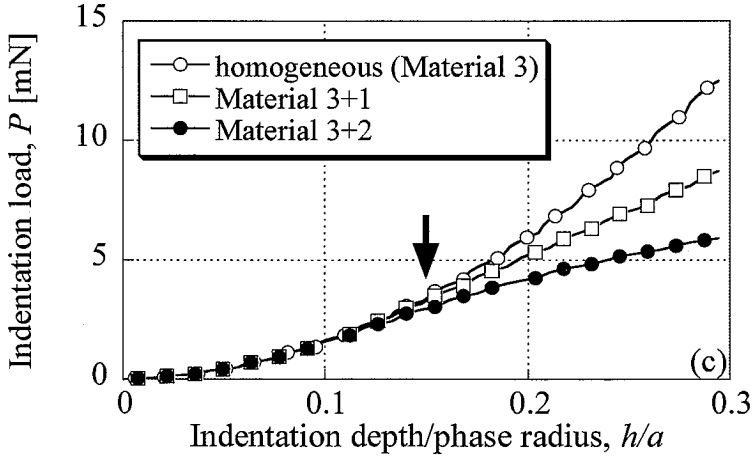

Fig. 4-9 Comparison of *P-h/a* curves between dual-phase and homogeneous models, where (a), (b) and (c) are cases when Material 1, 2 and 3 are chosen for indented material (Phase 1).

4.2.2 Identification of viscoplastic properties

A set of material parameters C and n in Eq. (4-1) for Sn-rich phase and Sn-Ag-Cu eutectic constituent in Sn-3.5Ag-0.75Cu lead free solder were identified by fitting the experimentally obtained P-h curves, as well as indentation-creep data, with the corresponding FE simulation results. Figs. (4-10) and (4-11) show the P-h curves for the two phases, respectively, obtained from micro-indentation experiments. In these figures, the corresponding FE simulation results incorporating with the thus identified set of material parameters are also indicated. Here, it is found that Sn-rich phase is harder than Sn-Ag-Cu constituent. For both phases, P-h responses and the subsequent indentation creep are strongly rate-dependent, *i.e.*, at higher speed (see Figs (4-10) (a) and (4-11) (a), $\dot{P} = 40$ mN/sec) the materials behave harder in loading process, and exhibit more significant creep, compared to the cases at lower speed (see Figs (4-10) (b) and (4-11) (b), $\dot{P} = 0.5$ mN/sec). From the material parameter identification, we found $C = 1.0\times10^{-20}$; $n = 10.5$ for Sn-rich phase and $C = 2.5\times10^{-23}$; $n = 11.0$ for Sn-Ag-Cu constituent. The calculated results for both phases agree well with the experimental data for loading processes and indentation creep.

4.2.3 Application of rule of mixture to determine the material parameters of bulk material

It would be interesting to know how precisely the bulk viscoplasticity behaviour can be predicted by using the rule of mixture in the composite theory based on the assumption of equal strain rate. From the theory, the following relationship between the viscoplastic strain rate $\dot{\varepsilon}^{vp}$ and applied stress σ_{bulk} is given as

$$\sigma_{bulk} = \sigma_0 \left[\left(\frac{\dot{\varepsilon}^{vp}}{C_1} \right)^{\frac{1}{n_1}} V_1 + \left(\frac{\dot{\varepsilon}^{vp}}{C_2} \right)^{\frac{1}{n_2}} V_2 \right] \tag{4-9}$$

where V_1 and V_2 denote the volume fraction of each phases, respectively. In Fig. (4-12), the relationship between viscoplastic strain rate and the applied stress calculated by Eq. (4-9), as well as the results for individual phases of Sn-rich phase and Sn-Ag-Cu eutectic constituent, are indicated. The experimental data obtained from compression tests with a bulk specimen of the same solder alloy are also plotted. The calculated results by Eq. (4-9) agree well with the experimental observation. Hence, it would be concluded that if mechanical properties and volume fraction of individual phase are prescribed, the bulk behaviour would be predicted by the rule of mixture.

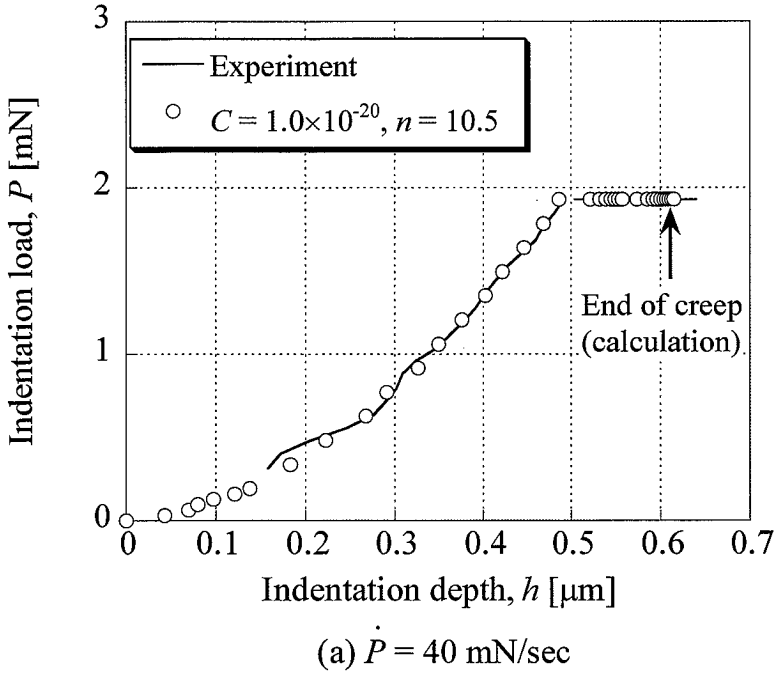

(a) $\dot{P} = 40$ mN/sec

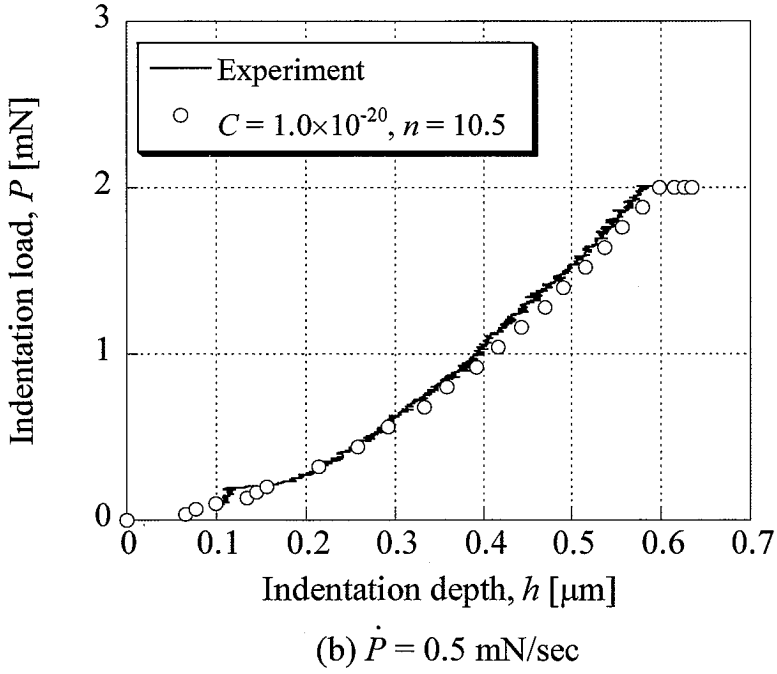

(b) $\dot{P} = 0.5$ mN/sec

Fig. 4-10 Comparison of *P-h* curves of Sn-rich phase between experimental data and FE simulation results incorporating with the identified set of material parameters; (a) for loading speed $\dot{P} = 40$ mN/sec and; (b) for loading speed $\dot{P} = 0.5$ mN/sec.

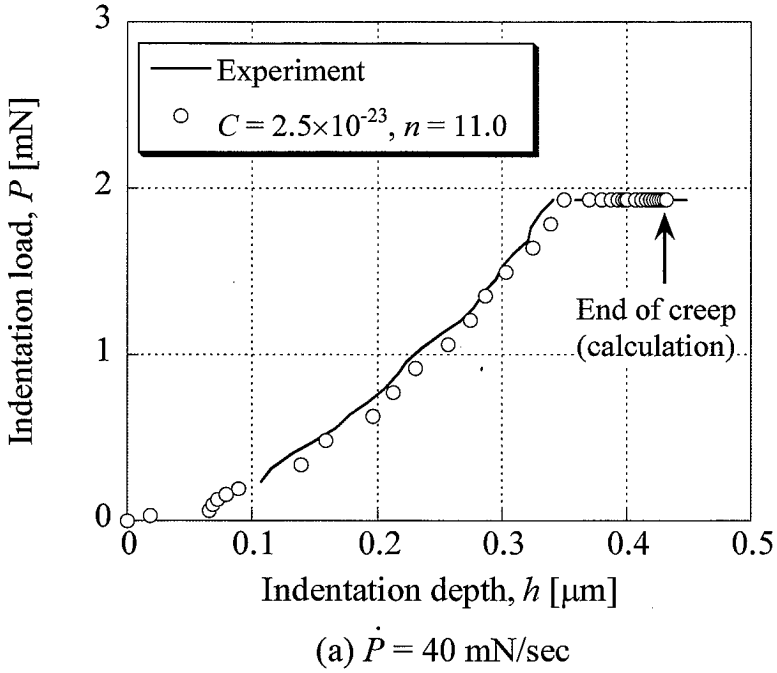

(a) $\dot{P}$ = 40 mN/sec

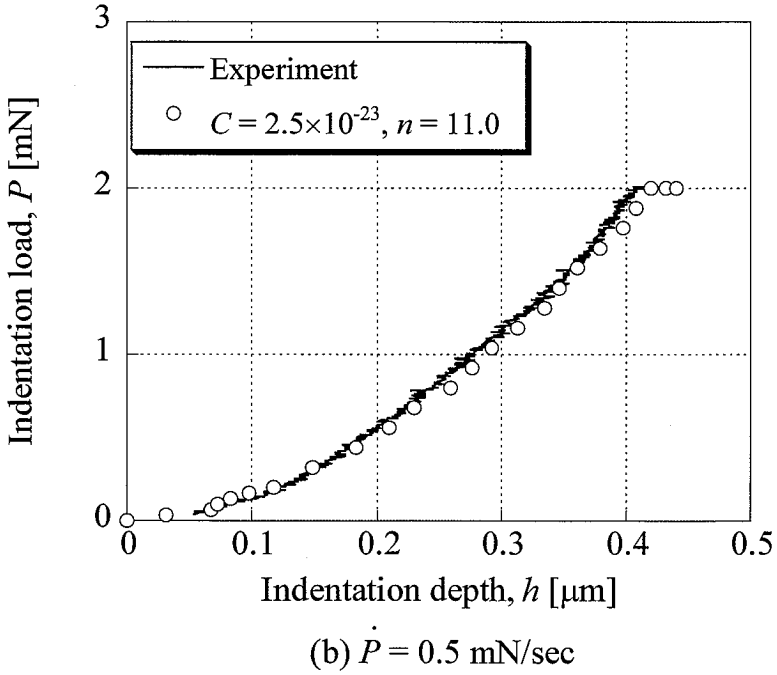

(b) $\dot{P}$ = 0.5 mN/sec

Fig. 4-11 Comparison of *P-h* curves of Sn-Ag-Cu eutectic constituent between experimental data and FE simulation results incorporating with the identified set of material parameters; (a) for loading speed $\dot{P}$ = 40 mN/sec and; (b) for loading speed $\dot{P}$ = 0.5 mN/sec.

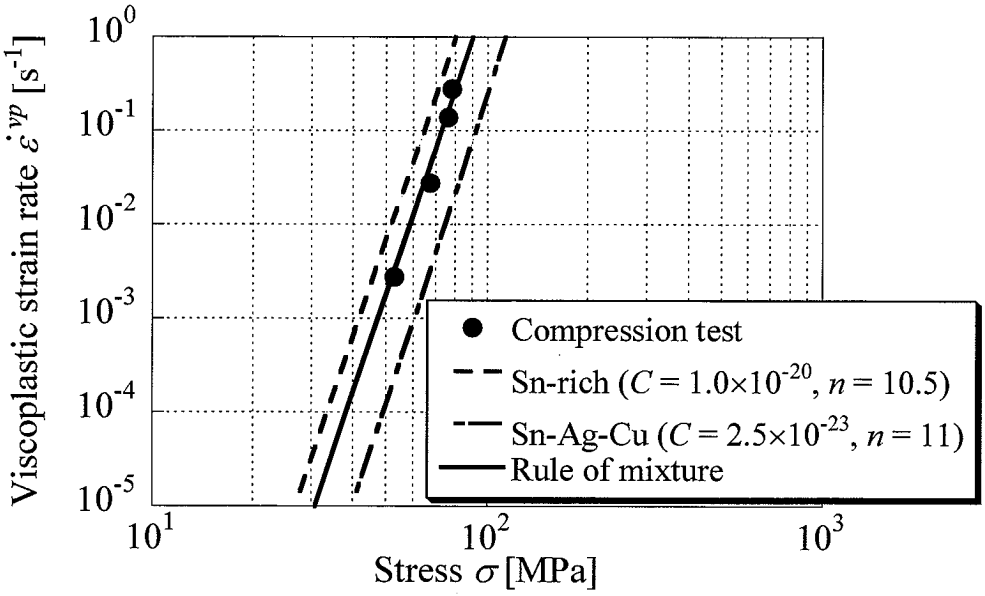

Fig. 4-12 Viscoplastic strain rate vs. stress relationship obtained from the compression test with bulk Sn-3.5Ag-0.75Cu lead-free solder (○), together with the calculated results by the rule of mixture (——) using the material parameters for Sn-rich phase (- - - -) and Sn-Ag-Cu eutectic constituent (- ——).

4.3 Conclusions

In this Chapter 4, a method of parameter identification for bulk and multi-phase materials of viscoplasticity is presented, and furthermore, it is verified by applying to Sn-3.5Ag-0.75Cu lead-free solder.

1. Sn-3.5Ag-0.75Cu lead-free solder shows a strong rate dependency on its *P-h* curve. In a case of high loading speed, progressive indentation creep is observed during a load-holding time, while almost no indentation creep appears in a case of low loading speed.
2. Even for Berkovich indentation, rate sensitivity characteristics of the lead-free solder strongly affect *P-h* responses. Therefore, in contrast to the case of plasticity parameter identification, any shapes of indenter can be applied on a viscoplasticity parameter identification.
3. Rate sensitivity exponent n and rate sensitivity coefficient C in Norton's law for the alloy were determined. Thus identified parameters shows a very good with the data obtained from uniaxial compression test.
4. From microscopic observation, it was found that Sn-3.5Ag-0.75Cu lead-free solder is mainly consists of Sn-rich phase and Sn-Ag-Cu eutectic constituent. To determine the viscoplastic parameters of individual phases of a dual-phase material, preferable indentation depth for Berkovich indentations, where *P-h* curve is not affected by the deformation of its neighboring phases, was determined by numerical experiments.
5. Viscoplasticity parameters of Sn-rich phase and Sn-Ag-Cu eutectic constituent were determined. An interesting result is that the strain rate vs. stress curve calculated by the rule of mixture, incorporating with

the identified set of viscoplasticity parameters for individual phases, shows a good agreement with the corresponding curve of compression test. This indicates that if the material parameters and volume fractions of individual phases are known, the stress-strain relationship of bulk material can be estimated by the rule of mixture.

References

[1] T. Ogawa, A. Miyamoto, K. Ohshimizu and T. Ohsawa : J. Soc. Mat. Sci., Japan, 49 (2000) 666-671 (in Japanese).

[2] A. Miyamoto, T. Ogawa and T. Ohsawa : J. Soc. Mat. Sci., Japan, 51 (2002) 445-450.

[3] M. Fujiwara and M. Otsuka : Mater. Sci. Eng., A319-321 (2001) 929-933.

[4] M. Fujiwara : J. JILM, 52 (2002) 282-290.

[5] P. M. Sargent and M. F. Ashby : Mater. Sci. Tech., 8 (1992) 594-601.

Chapter 5: Identification of plasticity properties of coating

For the development of high quality coated material, it is essential to determine the mechanical properties of coatings. However, this is not an easy task because the conventional mechanical tests, such as uniaxial tension and compression tests, are not applicable to thin coatings. Therefore, micro-indentation test has been often used to determine mechanical properties of coatings and thin films [1-3]. However, if the indenter-penetration depth is too deep, the *P-h* response will be strongly affected by deformation of substrates. Nevertheless, only limited papers [4-6] discussed the substrate effects on *P-h* curve for specific cases of the Berkovich indentation.

In this Chapter, the preferable indentation depth for a given coating thickness in Berkovich and spherical indentations, where the effect of deformation of substrates on *P-h* curve becomes negligibly small, is investigated. For plasticity parameter identification, the use of spherical indentation is recommended, since in self-similar indentations such as Berkovich indentation, *P-h* responses are insensitive to workhardening characteristics of materials. As an example, material parameters in Ludwik-type model of plasticity for Zn and Zn-Al coating placed on steel sheets were identified.

5.1 Guideline for indentation depth for coatings

5.1.1 Investigation of preferable indentation depth for coating by numerical experiments

For the identification of mechanical properties of coatings using micro/nano indentations, experimental data of *P-h* responses should not include the effect of the deformation of their substrates. To determine the preferable indentation depth h for a given coating thickness t_{coat}, numerical experiments were carried out for several model materials with different combinations of Young's modulus: E_{coat}/E_{sub} = 0.2, 1 and 5 (E_{coat} = 200 GPa), and yield strength: Y_{coat}/Y_{sub} = 0.1, 1, 5 and 10 (Y_{coat} = 200 MPa), where both coatings and substrates were assumed as elastic-perfectly plastic materials. The Berkovich indenter and a spherical indenter with the radius of 25 μm were employed. Fig. 5-1 shows the FE model of coating/substrate system with spherical indenter used for the numerical simulation. The deformation of substrates was evaluated by measuring strain component in indentation direction (z-direction) at the FE node existing just under the coating ε_z^{ref} (see the reference point in Fig. 5-1).

5.1.2 Results and Discussions

Figs. 5-2 (a) and 5-3 (a) show ε_z^{ref} vs. normalized indentation depth (h/t_{coat}) curves for the Berkovich and spherical indentations for various combination of yield strength of coating/substrate systems, and Figs. 5-2 (b) and 5-3 (b) are the corresponding *P-h* curves. Since the effect of Young's modulus differential is minor on *P-h* curves, especially in Berkovich indentation, only for a case of E_{coat}/E_{sub} = 1 is depicted in these figures. From the Berkovich indentation results (Fig. 5-2 (a)), it is clear that almost no deformation appears in the substrate until the indentation penetration reaches a certain amount of h/t_{coat} (refer to the arrow in Fig. 5-2 (a)) even for a case that the substrate is ten times softer than its coating (Y_{coat}/Y_{sub} = 10). Just after h/t_{coat}

exceeds 0.1, the deformation of substrate begins and increases when a coating is considerably harder than its substrate ($Y_{coat}/Y_{sub} \geq 5$), while still almost no strain appears for cases of softer coatings ($Y_{coat}/Y_{sub} \leq 1$).

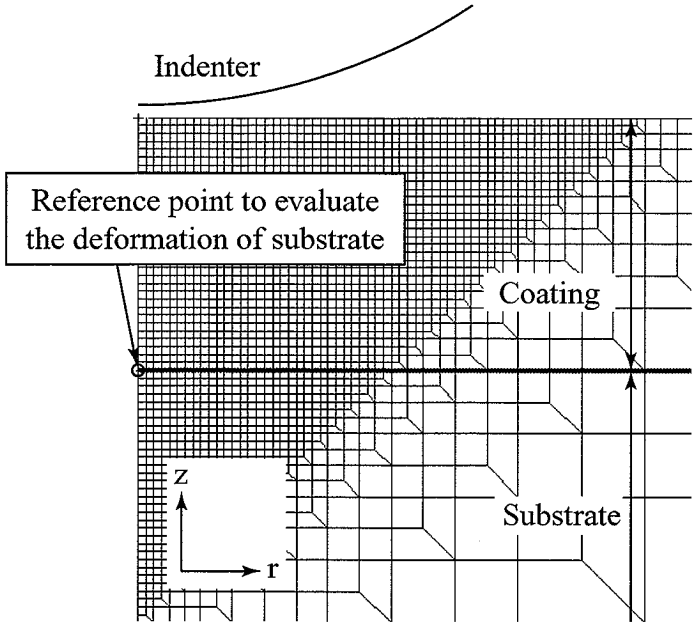

Fig. 5-1 FE model of an indentation for coating/substrate system.

Contrary to the Berkovich indentations, substrates deform at the very early stages of indentation for spherical indentations (see Fig. 5-3 (a)) for $Y_{coat}/Y_{sub} \geq 5$. Even for a case of $Y_{coat}/Y_{sub} = 1$, which means coating/substrate system is not the layered but homogeneous material, strain at the reference point increases from the beginning of indentation.

When a coating is harder than its substrate, *P-h* responses (see Figs. 5-2 (b) and 5-3 (b)) are strongly affected by the deformation of substrates, for both Berkovich and spherical indentations, while almost no effect is found for the opposite case of coating/substrate strength differential. However, in Berkovich indentation, it should be noted that, even for hard-coating/soft-substrate systems, the substrate effect is minor until the indentation penetration reaches 10 % of the coating thickness.

5.1.3 Workhardening parameter identification for layered material

As already mentioned in Chapter 3, it is impossible to identify the workhardening parameters in constitutive model of a material from the Berkovich indentation. For a case of a layered material, since the effect of substrate is minor on *P-h* curve for the Berkovich indentation when the indentation depth is up to 10 % of coating thickness, it is again invalid to obtain the plasticity parameters for coating from the Berkovich indentation. For example, Fig. 5-4 (a) shows the calculated *P-h* responses in Berkovich indentations for two models materials, one is a perfectly-plastic material and the other a workhardening material of Ludwik type ($\sigma = 80 + 500(\varepsilon^p)^{0.5}$ MPa). These two *P-h* curves show almost the same responses

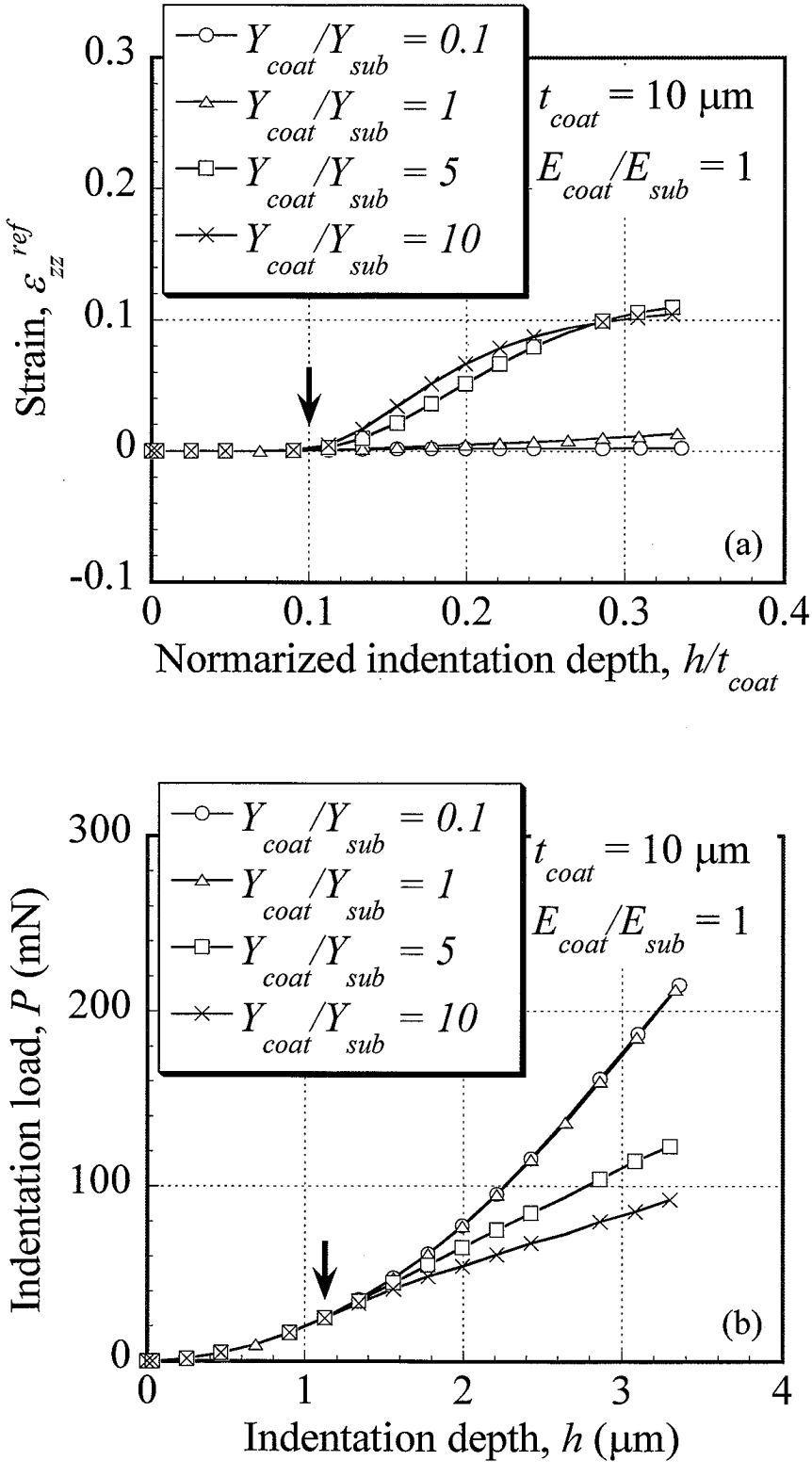

Fig. 5-2 FE simulation results for Berkovich indentation: (a) strain of substrates at the reference point just under the coatings: (b) those corresponding *P-h* curves.

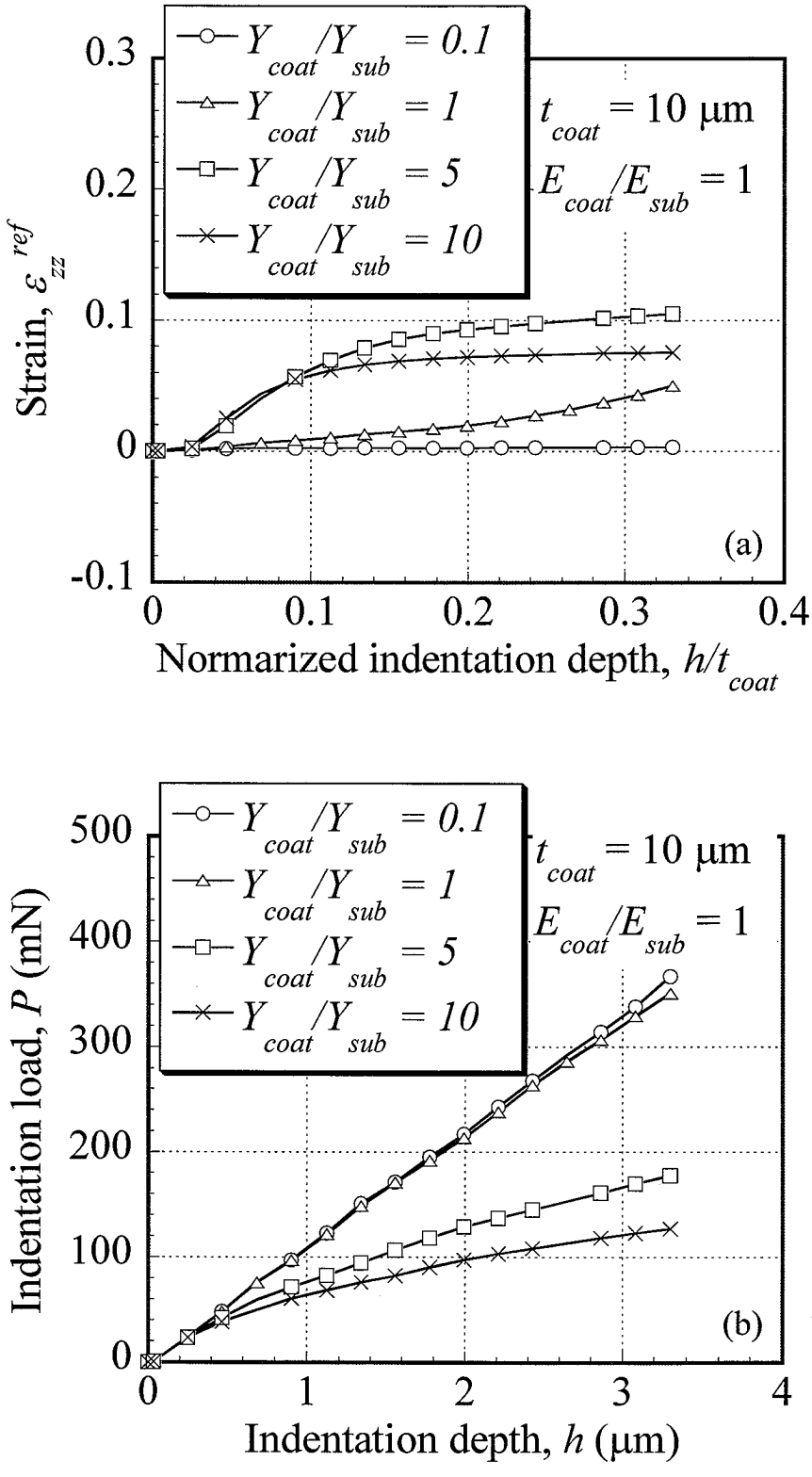

Fig. 5-3 FE simulation results for spherical indentation: (a) strain of substrates at the reference point just under the coatings: (b) those corresponding *P-h* curves.

although the workhardening characteristics are completely different (see Fig 5-4 (b)). Contrary to this, in spherical indentation, the difference in workhardening of materials reflect directly to *P-h* curves, as shown in Fig. 5-4 (a). From the above results, it can be concluded that spherical indentation is suitable for workhardening parameter identification. However for a coating/substrate system, as already mentioned, in the previous section, the substrate effect on *P-h* responses is dominant in spherical indentation. Hence for the identification of plasticity properties of a coating by spherical indentation, the properties of substrate must be obtained in advance. This is not a difficult problem, since usually a substrate is much thicker than its coating, and the determination of plasticity properties of the substrate is possible by spherical indentation.

5.2 Micro-indentation experiments on Zn and Zn-Al coatings

5.2.1 Specimens and experimental conditions

Micro-indentation tests were performed on two types of coatings, Zn (99.6 wt%-Zn) and Zn-Al (51.4-Al/45.2 wt%-Zn), on steel sheets. The thickness of Zn and Zn-Al coatings were 24 and 21 μm, respectively (see Fig 5-5), where for both specimens the thickness of steel substrates was 0.5 mm. Two types of indenters (one is Berkovich indenter and the other a spherical indenter with the radius of 25 μm) were selected to observe the *P-h* responses. Table 5-1 shows the experimental conditions. For Berkovich indentation, loading speed of 0.5 mN/s, maximum load of 250 mN, 1 second holding time and 5 second unloading time were selected, while loading speed of 7 mN/s, maximum load of 700 mN, 1 second holding time and 5 second unloading time were used for spherical indentation.

5.2.2 Results and discussion

Figs. 5-6 (a) and 5-7 (a) show the obtained *P-h* curves of Zn and Zn-Al coatings for Berkovich indentations respectively. In both figures, two *P-h* curves, which were performed on different points of the same specimen, are compared. For the case of indentation on Zn-Al coating, since the coating is a composite material mainly consisting of Zn-, Al- and Si-rich phases, *P-h* responses depend on indented points of the coating, while two *P-h* curves traced almost the same course for the case of Zn coating. Figs. 5-6 (b) and 5-7 (b) are the *P-h* responses of Zn and Zn-Al coatings for spherical indentations, respectively. Here, again two *P-h* curves, which were obtained from the different indentation points of the same specimens, were compared. In contrast to the Berkovich indentations for Zn-Al coating (Fig 5-7 (a)), two *P-h* curves show a good agreement even for a composite surface of Zn-Al (Fig 5-7 (b)). This is because, numbers of phases of Zn-Al coating was plastically deformed by the spherical indenter under the maximum load of 700 mN, and as a result, *P-h* responses in spherical indentation always show an average responses of the coating material.

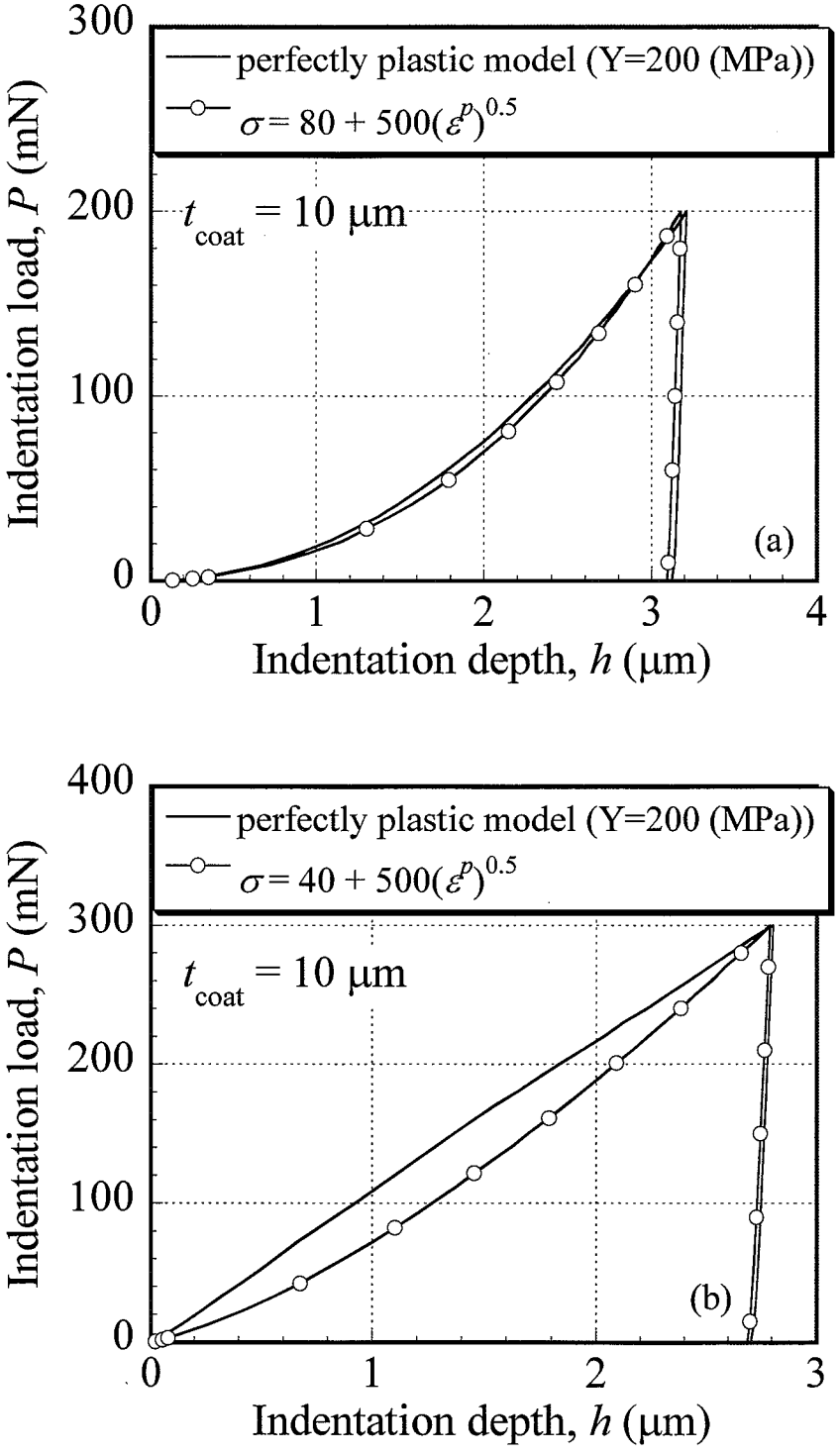

Fig. 5-4 Comparison of *P-h* curves calculated for a perfectly-plastic material and a workhardening material of Ludwik type, where (a) Berkovich indentation; and (b) spherical indentation.

Table 5-1 Experimental conditions.

coating material	indenter	maximum load (mN)	loading speed (mN/s)	holding time (s)	unloading time (s)
Zn and	Berkovich	250	0.5	1	5
Zn-Al	spherical	700	7	1	5

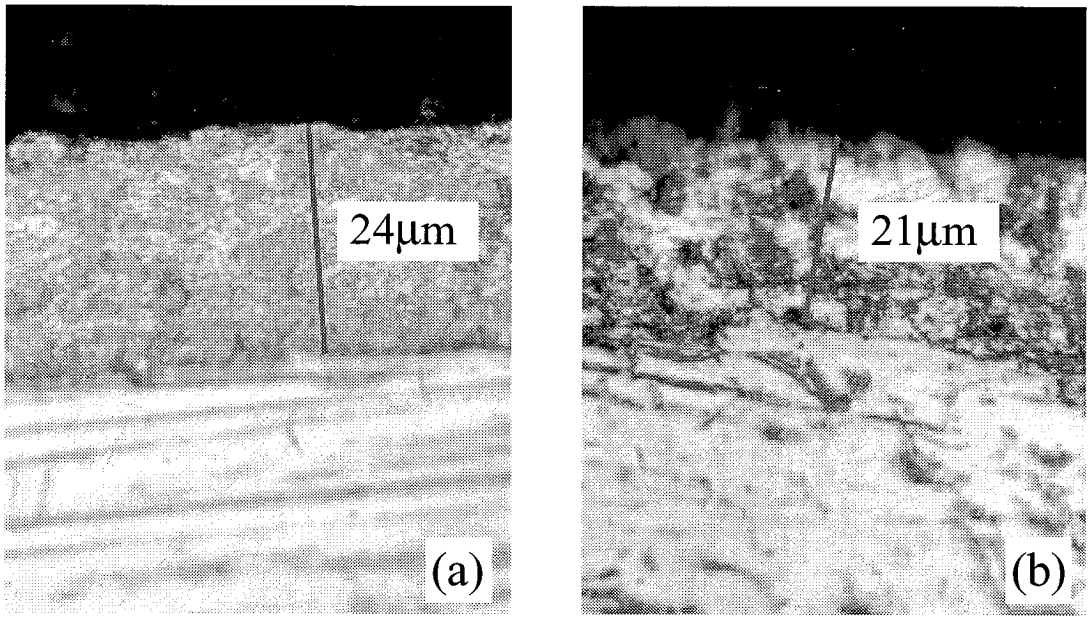

Fig. 5-5 Microscopic observations of coating thicknesses; (a) Zn; anc (b) Zn-Al coatings.

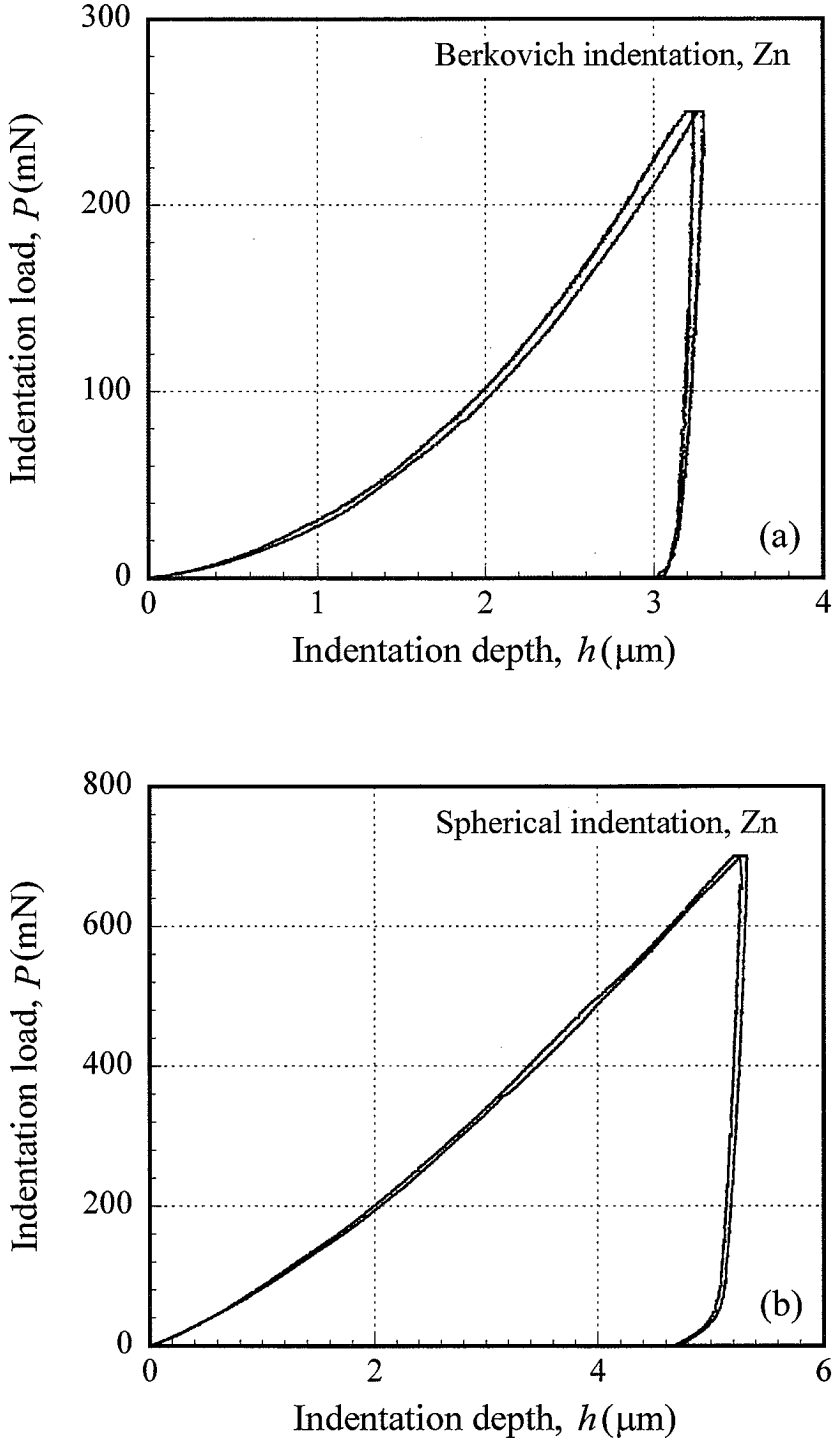

Fig. 5-6 *P-h* curves obtained from micro-indentation for Zn coating; (a) for Berkovich indentations; and (b) spherical indentations.

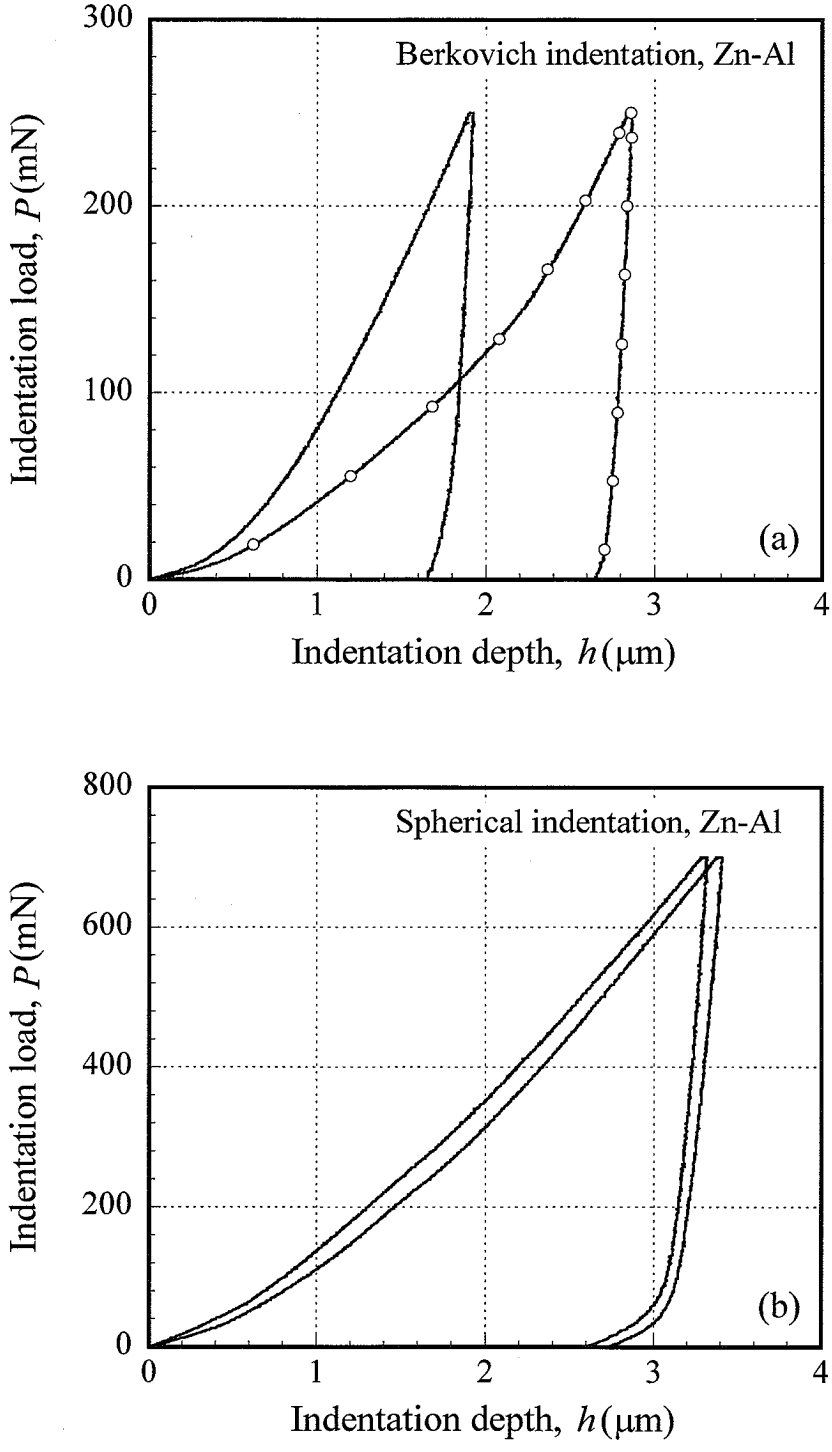

Fig. 5-7 *P-h* curves obtained from micro-indentation for Zn-Al coating; (a) for Berkovich indentations; and (b) spherical indentations.

5.3 Plasticity parameter identification for Zn and Zn-Al coatings

For the parameter identification, the Ludwik type stress-strain relationship is assumed for both of coating:

$$\sigma = Y + C\left(\varepsilon^{p}\right)^{n} \tag{5-1}$$

where Y, C, n are the material parameters to be identified, which denote initial yield strength, workhardening coefficient and workhardenign exponent, respectively. Since elasticity parameters were insensitive to P-h response, Young's modulus and Poisson's ratio were assumed 100 GPa and 0.3 for Zn coating, and 50 GPa and 0.3 for Zn-Al coating, respectively. Since the deformation of substrate steel sheet was expected to be minor, it was assumed to be elastic-perfect-plastic materials with the value of 320 and 350 GPa for Zn and Zn-Al coatings, respectively. Figs.5-8 and 5-9 show experimental P-h curves and the corresponding results of FE simulations incorporating with thus identified set of plasticity parameters for Zn and Zn-Al coatings. From P-h curve fitting, yield strength Y, workhardening coefficient C and workhardening exponent n were determined as 90 MPa, 500 MPa and 0.5 for Zn coating, and 200 MPa, 800 MPa and 0.4 for Zn-Al coating, respectively.

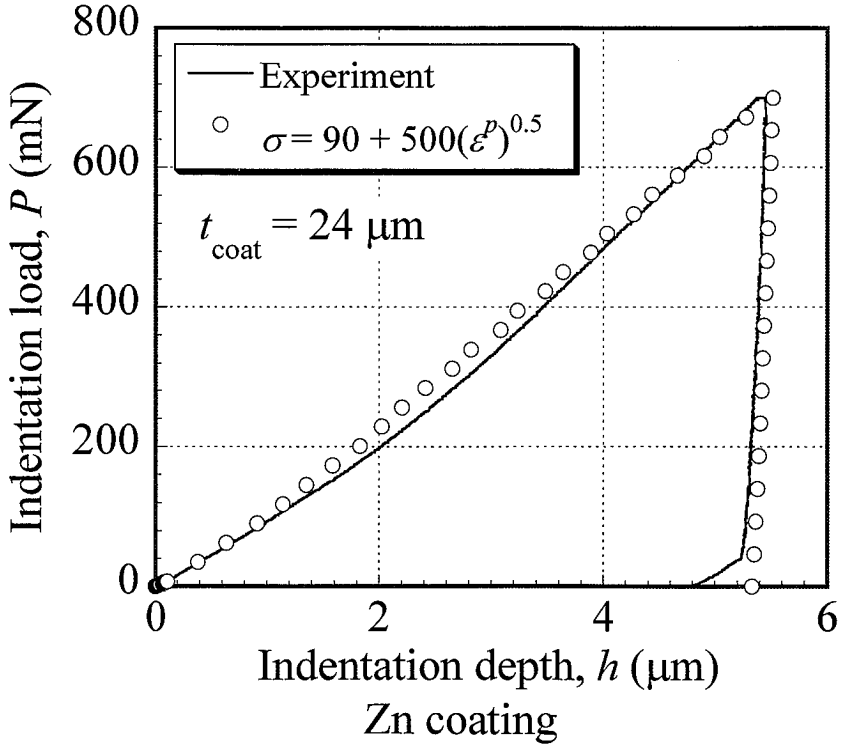

Fig. 5-8 Experimental P-h curve for Zn coated steel sheet and the corresponding FE simulation result incorporating with the identified set of material parameters.

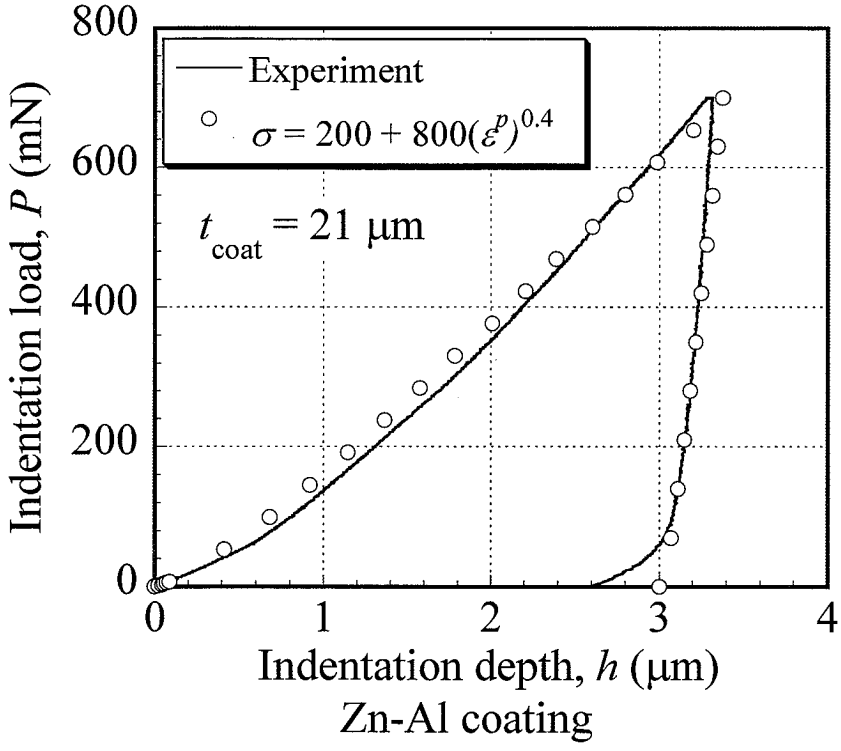

Fig. 5-9 Experimental *P-h* curve for Zn-Al coated steel sheet and the corresponding FE simulation result incorporating with the identified set of material parameters.

5.4 Conclusions

In the present work, a method of plasticity parameter identification for metallic coatings using depth-sensing micro-indentation experiment and FE simulation was presented. The present findings are summarized as follows:

1. When a coating is harder than its substrate, deformation of substrate affects *P-h* response significantly. On the other hand, in the opposite cases of coating/substrate strength differential, the substrate effect is minor.

2. In the Berkovich indentation, the effect of deformation of substrate can be ignored when the indentation penetration depth is less than 10 % of coating thickness, while in spherical indentation, the substrate deforms at the very early stage of indentation.

3. For plasticity parameter identification, spherical indentation is necessary, since in self-similar indentations such as Berkovich indentation, *P-h* responses are insensitive to workhardening characteristics of materials.

4. An inverse approach for the identification of plasticity properties using indentation experimental data has been proposed, and using this, Zn and Zn-Al coatings on steel sheets were successfully determined.

References

[1] R. Nowak, F. Yoshida, J. Morgiel and B. Major : J. Appl. Phys., 85 (1999) 841-852.

[2] R. Nowak, M. Pessa, M. Suganuma, M. Leszczynski and F. Yoshida : Appl. Phys. Lett., 75 (1999) 2070-2072.

[3] G. Yu, H. Ishikawa, T. Egawa, T. Soga, J. Watanabe, T. Jimbo and M. Umeno : J. Crys. Growth., (1998) 701-705.

[4] D. Lebouvier, P. Gilormini and E. Felder : J. Phys. D : Appl. Phys., 18 (1985) 199-210.

[5] D. Lebouvier. P. Gilormini and E. Felder : Thin Solid Films, 172 (1989) 227-239.

[6] Y. Sun, T. Bell and S. Zheng : Thin Solid Films, 258 (1995) 198-204.

Chapter 6: Conclusions

In this thesis has presented the material parameter identification system using depth-sensing micro-indentation, FE simulation and optimization, and discuss its applications for several materials. To achieve material parameter identification automatically and systematically, an inverse analysis based on optimization technique for *P-h* curve fitting is employed. The guidelines for the choice of indenter shape and indenter-penetration depth have been proposed for several elasto-plasticity and viscoplasticity materials, multi-phase materials and coatings. This thesis is composed of six chapters. Important findings, new propositions and some remarks of each chapter are summarized as follows:

In Chapter 1, reviewing the previous research works, some problems of material parameter identification using depth-sensing micro-indentation, which have not been explicated so far, are pointed out. The purpose and the outline of the present research are presented.

In Chapter 2, the concept and the procedure of material parameter identification using depth-sensing micro-indentation, FE simulation and optimization have been presented. This technique has the following features:

(1) An inverse approach, where FE simulation is iteratively performed by correcting a set of material parameter until its *P-h* curve fits well to the corresponding experimental result, is presented.
(2) For material parameter identification, appropriate indenter type should be selected depending on material characteristics of a specimen. For example, Berkovich indentation, namely self-similar indentation, is not capable to identify workhardening parameter of plasticity so that the spherical indenter should be chosen in this case.
(3) To perform the material parameter identification process systematically, an optimization technique is introduced. This optimization software automatically changes a set of material parameters in FE simulation iteratively and efficiently finds an optimal solution.
(4) The validation of the proposed method is confirmed by applying it for a mild steel sheet. As a result, stress-strain curve, which is calculated by Ludwik type of constitutive model incorporating with the identified material parameters, shows a good agreement with the uniaxial tension test result.

In Chapter 3, details of optimization technique employed for an inverse approach are described. Significant features of this methodology is as follows:

(1) Multi-point approximation methodology based on response surface fitting (MARS) is adopted to calculate the optimal solution. This technique allows us to reduce the whole computing time to solve the optimization problem, since FE simulation is performed only for building an approximation function of the objective function.
(2) The squared deviation of *P-h* curve calculated by FE simulation from the corresponding experimental

result is employed as the objective function to minimize the difference of these curves. When both two *P-h* curves are completely the same, objective function value will be zero, while this value increases as difference of two curves increases.

(3) Even though MARS requires less number of FE simulations than conventional optimization technique, FE simulation itself needs a large amount of time even for a single simulation. Therefore, only low-fidelity FE model, which means a model consists of coarser mesh, is used during optimization process. To keep the accuracy corresponding to the high-fidelity model, the objective function value obtained from the result of low-fidelity model is corrected by the simple equation which is build from the numerical experiments to interacts the low- and high-fidelity models. The computing time for the material parameter identification process is dramatically reduced by adopting this method.

In Chapter 4, a method of parameter identification for bulk and multi-phase materials of viscoplasticity is presented, and furthermore, it is verified by applying to Sn-3.5Ag-0.75Cu lead-free solder.

(1) Sn-3.5Ag-0.75Cu lead-free solder shows a strong rate dependency on its *P-h* curve, In a case of high loading speed, progressive indentation creep is observed during a load-holding time, while almost no indentation creep appears in a case of low loading speed.

(2) Even for Berkovich indentation, rate sensitivity characteristics of the lead-free solder strongly affect *P-h* responses. Therefore, in contrast to the case of plasticity parameter identification, any shapes of indenter can be applied on a viscoplasticity parameter identification.

(3) Rate sensitivity exponent n and rate sensitivity coefficient C in Norton's law for the alloy were determined. Thus identified parameters shows a very good with the data obtained from uniaxial compression test.

(4) From microscopic observation, it was found that Sn-3.5Ag-0.75Cu lead-free solder is mainly consists of Sn-rich phase and Sn-Ag-Cu eutectic constituent. To determine the viscoplastic parameters of individual phases of a dual-phase material, preferable indentation depth for Berkovich indentations, where P-h curve is not affected by the deformation of its neighboring phases, was determined by numerical experiments.

(5) Viscoplasticity parameters of Sn-rich phase and Sn-Ag-Cu eutectic constituent were determined. An interesting result is that the strain rate vs. stress curve calculated by the rule of mixture, incorporating with the identified set of viscoplasticity parameters for individual phases, shows a good agreement with the corresponding curve of compression test. This indicates that if the material parameters and volume fractions of individual phases are known, the stress-strain relationship of bulk material can be estimated by the rule of mixture.

In Chapter 5, a method of plasticity parameter identification for metallic coatings using depth-sensing micro-indentation experiment and FE simulation was presented. The present findings are summarized as follows:

(1) When a coating is harder than its substrate, deformation of substrate affects *P-h* response significantly. On the other hand, in the opposite cases of coating/substrate strength differential, the substrate effect is minor.

(2) In the Berkovich indentation, the effect of deformation of substrate can be ignored when the indentation penetration depth is less than 10 % of coating thickness, while in spherical indentation, the substrate deforms at the very early stage of indentation.

(3) For plasticity parameter identification, spherical indentation is necessary, since in self-similar indentations such as Berkovich indentation, *P-h* responses are insensitive to workhardening characteristics of materials.

(4) An inverse approach for the identification of plasticity properties using indentation experimental data has been proposed, and using this, Zn and Zn-Al coatings on steel sheets were successfully determined.

In Chapter 6, the conclusions and some remarks in the present work are summarized.

As summarized above, this thesis has proposed a novel approach to the identification of material parameters of elaso-plasticity and viscoplasticity by means of depth-sensing micro-indentation, FE simulation and optimization technique. Guidelines for selection of indenter type and appropriate indenter-penetration depth have been established through numerical simulations and experiments. Here, it should be emphasized that the present approach is highly original, and it has a great advantage over other methods so far proposed in obtaining accurate material parameters within an acceptable computation time. Hence, this technique of material parameter identification is beneficial for the development of micro technologies, such as micro-joining, micro-fabrications, MEMS etc..

Acknowledgments

First and foremost, I would like to thank Prof. Fusahito Yoshida. Throughout my doctor course in Hiroshima University, he has acted as my advisor, mentor and supporter for making me achieve better research results. He taught me much how to analysis things and overcome difficulties met during my research period and how to answer to the reviewer comments of my paper submitted to the journals.

I would also like to thank Prof. Toshiyuki Sawa, Yasuo Yamane and Prof. Ryutaro Hino for their valuable advises and comments on my researches.

My profound gratitude is also extended to Prof. Roman Nowak (Helsinki University of Technology), Prof. Vassili V. Toropov (Altair Engineering), Asistant Takeshi Uemori and Dr. Luis F. Alvarez (Univerisity of Bradford) for their much helping and encouragement in the period of my research in Hiroshima Univeristy.

I am also grateful to Prof. Tetsuo Naka (Yuge National College of Maritime Technology), Prof. Michihiro Takiguchi (Hiroshima National College of Maritime Technology) and Prof. Tetsuya Yoshida (Hiroshima National College of Maritime Technology) for their kind helping in the specimens's making.

Last, I would like to thank Mr. Kazuhiro Shinbata, Seiji Matsumoto, Tetsuya Nakamura, Takumi Inoue and whole members of Elasto-plastic laboratory for their friendly cooperation.